

Gust-Front Factor

Dae-Kun Kwon¹, Ahsan Kareem²

ABSTRACT

In comparison with atmospheric boundary layer winds, which are customarily treated as stationary, winds associated with gust-fronts originating from a thunderstorm/downburst exhibit rapid changes during a short time period which may be accompanied by changes in direction. This introduces nonstationarity both in the mean and the standard deviation of wind fluctuations. In order to realistically capture characteristics of gust-front winds and their attendant load effects, a new analysis framework is presented which is named here as the gust-front factor approach. This is akin to the gust loading factor format used in codes and standards world-wide for the treatment of conventional boundary layer winds. The gust-front factor expresses a generalized description of the genesis of the overall wind load effects on structures under both gust-front and boundary layer winds and it reduces simply to the gust loading factor for the case of conventional boundary layer winds. This approach encapsulates both the kinematic and dynamic features of gust-front induced wind effects on structures which distinguish themselves from those experienced in conventional boundary

¹ Postdoctoral Research Associate, Dept. of Civil Engineering and Geological Sciences, Univ. of Notre Dame, Notre Dame, IN 46556. E-mail: dkwon@nd.edu

² Robert M. Moran Professor, Dept. of Civil Engineering and Geological Sciences, Univ. of Notre Dame, Notre Dame, IN 46556. E-mail: kareem@nd.edu

layer flows, i.e., variation in the kinematics of the velocity profile and its effects on the associated aerodynamics; dynamic effects induced by the sudden rise in wind speed; non-stationarity of turbulence in gust-front winds; transient aerodynamics.

To facilitate expeditious utilization of this framework in design practice and inclusion in codes and standards, the analysis framework and its workflow is introduced within a web-based portal. This eliminates the need for an in-depth understanding of the background within the framework and the need for associated computational effort. The portal has a user-friendly interface which is available at <http://gff.ce.nd.edu>, permitting convenient analysis of several design scenarios with a host of potential loading conditions including the current ASCE 7-05 procedure in boundary layer winds for immediate comparison.

CE Database subject headings: Wind Gusts; Wind Loads; Building design; Structural Response; Nonstationary Process; Building codes; Gust loading factor; Thunderstorm; ASCE 7; Information technology (IT)

INTRODUCTION

Due to spatio-temporal fluctuations in boundary layer winds, the dynamic effects of winds on structures have been of major concern in structural engineering. To account for the gustiness of the turbulent boundary layer wind in structural loading, most international codes and standards have adopted the concept of a gust loading factor which was first introduced by Davenport (1967) and has been extensively examined by a host of researchers (e.g., Solari 1993a, b; Simiu and Scanlan 1996) and more recently recast into a new format by Zhou and Kareem (2001). In comparison with boundary layer winds that have generally been regarded as stationary, gust-front winds that result from a thunderstorm/downburst exhibit distinct nonstationarity, i.e., rapid changes in wind speed during a short time interval. The significance of these transient wind events, as they relate to subsequent load effects, can be readily surmised based on the analysis of thunderstorm databases both in the U.S. and around the world, which suggest that these winds actually represent the design wind speed for many locations.

The mechanics of gusts associated with convective gust-fronts differs significantly from traditional turbulence in boundary layer winds both in its kinematics and dynamics. The key distinguishing attributes are the contrasting velocity profile with height, a rapid increase in speed and the statistical features of the energetic gusts in the wind field. In gust-fronts, the traditional velocity profile does not exist; rather it bears an inverted velocity profile with its maxima near the ground potentially exposing low- to mid-rise structures to higher wind loads. Furthermore, such a change in the approach flow profile/kinematics, even in a steady state flow, would introduce a major change in the flow-structure

interaction that may differ significantly from the corresponding boundary layer flow case. This is compounded by the inherent transient nature of energetic convective gusts that rapidly increase in amplitude and direction, raising serious questions regarding the applicability of conventional aerodynamic loading theories. The nonstationarity is the critical issue in these wind events, which has been examined utilizing full-scale measurements (e.g., Chen and Letchford 2005a, b; Choi 2001; Wang and Kareem 2004, 2005; Xu and Chen 2004).

Thus, design loads in gust-front winds obtained from conventional analysis frameworks included in codes and standards, such as the gust loading factor approach (ASCE 7), may not be appropriate, calling for a careful examination of traditional design procedures. In an effort to establish a new procedure for this type of wind load effect on structures, this study introduces a gust-front factor based framework that accounts for the changes in load effects in gust-front winds. The gust-front factor, akin to the gust loading factor for boundary layer winds found in many codes and standards, is designed to be used in conjunction with the existing design standards, ASCE 7 (Kareem et al. 2006; Kwon and Kareem 2007). To facilitate expeditious utilization of this framework in design practice, a web-based portal for the evaluation of gust-front factor and associated loads is available at <http://gff.ce.nd.edu>.

It is envisioned that the proposed gust-front factor framework would benefit from further refinements over time, as additional knowledge about the gust-front wind field and associated interactions with structures are better understood, like many subsequent developments to date that have occurred to gust loading factor approach since its introduction in 1967. In the absence of any procedure to quantify the effect of gust-front

winds on structures to date, this scheme offers an effective framework to capture, in a rational manner, the influence of various distinctive features of gust-fronts on structures based on the current state-of-the-art.

MODEL OF GUST-FRONT WINDS

In this study, analytical/empirical models of downburst winds that characterize their spatio-temporal features are employed. For mathematical convenience, it is generally assumed that gust-front wind field at any time and height may be factorized in terms of the product of a vertical profile and a time function, e.g.,

$$V_{G-F}(z, t) = V_{G-F}(t) \cdot V_{G-F}(z) \quad (1)$$

where, subscript $G-F$ = gust-front wind; $V_{G-F}(z)$ = vertical profile of gust-front wind; $V_{G-F}(t)$ = normalized time function of gust-front wind (e.g. Chen and Letchford 2004a, b; Chay and Albermani 2005; Chay et al. 2006). This separable type description is an adequate representation of the velocity field in light of rather limited full-scale observations and its success in modeling similar nonstationary physical processes. Certainly, this model may be modified if additional data suggest an alternate description.

Time function, $V_{G-F}(t)$

The time function describes the time-varying mean of the wind speed in nonstationary winds. One can derive models based on actual measurements, e.g., the Andrews AFB downburst, which has been well documented due to its highest observed wind speed of 67 m/s (149. mph) at 5 m (16 ft) in a short time interval (e.g., Fujita 1985, 1990). Another

example of full-scale downburst data involves rear-flank downdraft (RFD) and Derecho data which has been obtained in the 2002 thunderstorm outflow field experiment (Gast and Schroeder 2003). Fig. 1(a) shows wind record of the Andrew AFB downburst (Fujita 1985), which has been employed in several previous studies to examine the time-varying feature of gust-front and the gust-front induced load effects (e.g., Holmes and Oliver 2000; Chen and Letchford 2004a). It has two distinct peaks, the first being very large followed by a relatively small peak, which represents the passage of a downburst over the measurement position. In Fig. 1(b), a sample of the RFD data measured from Tower 4 at 10 m height is shown (Gast and Schroeder 2003) and its wavelet-based extraction of time-varying mean are plotted (Wang and Kareem 2004). Similar to the Andrew AFB downburst record (Fig. 1a), the RFD data (Fig. 1b) also contains a very large peak followed by a small peak, and its peak lasted approximately 2~3 min from wind speed rise to fall, which is a relatively short time event compared to the typical 1-hour time period used in establishing the mean wind speed in typical boundary layer winds. In Figs. 1(a) and (b), it is observed that one large peak is a common feature in observed gust-fronts which may potentially be responsible for causing enhanced loads on the structure.

Rather than relying on the time-varying features of only a few storms records to represent the transient nature of the storm, for generality, this study employs a half-sine wave to describe this feature. Even though it may not represent the exact time variation of winds in a gust-front, it captures the underlying feature potentially responsible for enhanced loads. At a future time, this description may be revised once a sufficient number of measurements becomes available and an acceptable description of this function is arrived at based on an ensemble average of such observations. In this study the function is defined as

$$V_{G-F}(t) = \sin\left(\frac{\pi}{t_d} t\right) \quad (2)$$

where, t_d = pulse duration of the excitation. The simplicity of expression is an attractive feature as it requires only a single parameter, t_d , to define the time function in a gust-front wind event as shown in Fig. 1(c), while encapsulating the essential features of a sudden rise and drop in wind speed.

Vertical profile, $V_{G-F}(z)$

The vertical profile of gust-front winds is critical in evaluating the wind effects on structures, however, very limited full-scale data along the height is available to identify and reliably establish a description of the vertical profile (e.g., Oseguera and Bowles 1988; Hjelmfelt 1988). Several analytical/empirical models to describe the vertical profile of gust-front winds have been proposed based on limited full-scale measurements (e.g., Oseguera and Bowles 1988; Vicroy 1991, 1992). It is noted that in gust-fronts, the traditional velocity profile does not exist; rather it bears an inverted velocity profile with its maxima near the ground, giving it a “nose-shape” vertical profile (e.g., Fig. 2). This profile has also been studied in laboratory scale experiments by employing different mechanisms, e.g., by impinging jets on wall (e.g., Alahyari and Longmire 1995; Yao and Lundgren 1996; Wood et al. 2001; Chay and Letchford 2002; Letchford and Chay 2002; Choi 2004; Xu and Hangan 2005), by introducing a plate/flap suddenly in the flow (e.g., Butler and Kareem 2007), by individually controlling multiple fan wind tunnels (e.g., Kikitsu et al. 1999; Cao et al. 2002; Butler and Kareem 2007), by introducing a wall jet (e.g., Lin and Savory 2006)

or shutter mechanism (e.g., Matsumoto et al. 2007) in a wind tunnel stream, or by utilizing computational fluid dynamics (CFD) (e.g., Wood et al. 2001; Hangan et al. 2003; Chay et al. 2006; Kim and Hangan 2007; Mason et al. 2007).

It has been generally accepted that the vertical profile of the gust-front changes with time due to the translation of the storm, however, in the absence of full-scale data the modeling of this complex, time-variant vertical profile has been deferred in this study until more reliable information becomes available to model the profile. Since the time function (2) is normalized with unit amplitude, wind speed in a gust-front wind is described in the vertical profile. From a practical viewpoint, the worst scenario for wind loads on structures may be the highest wind speed which occurs at about one downdraft jet diameter from its point of impact (Hjelmfelt 1988). In this study, without loss of generality, the following model proposed in Vicroy (Vicroy 1991, 1992) is utilized:

$$V_{G-F}(z) = A \cdot V_{max} \left[e^{b_1(z/z_{max})} - e^{b_2(z/z_{max})} \right] \quad (3)$$

where, V_{max} = maximum horizontal wind speed, z_{max} = a height where V_{max} occurs, A = a constant that can be determined from model constants b_1 and b_2 . Note that Vicroy recommended model constants of $b_1 = -0.22$ and $b_2 = -2.75$ (Vicroy 1991), however, those were modified to $b_1 = -0.15$ and $b_2 = -3.2175$ in Vicroy (1992) without any specific explanation. Accordingly, constant A (3) has two values: 1.354 (1991) and 1.219 (1992) depending on the model constants (b_1 and b_2). Both versions have almost the same trend below z_{max} , while some variation is noted above z_{max} .

It is worth noting that the Vicroy model (3) based on the Terminal Area Simulation System (TASS) model derived from full-scale data of the Joint Airport Weather Studies (JAWS) (Oseguera and Bowles 1988) includes the following implicit relationship.

$$\frac{z_{max}}{z^*} = 0.22 \quad (4)$$

where, z^* = a characteristic length scale associated with the region “out of boundary layer” (above z_{max}), the height at which wind speed is half of the maximum wind velocity ($0.5V_{max}$). Substituting z^* (4) in Eq. (3) results in $V_{G-F}(z^*)$ equal to $0.50V_{max}$ in the 1991 model, while $0.62V_{max}$ in the 1992 model. Based on this observation, the 1991 model may be a more reasonable estimate to agree with the z^* definition, i.e., $V_{G-F}(z^*) = 0.50V_{max}$. Therefore, the following model constants in the Vicroy model (3) are finally selected for this study: $A = 1.354$, $b_1 = -0.22$ and $b_2 = -2.75$.

Criteria for profile comparison in gust-front and boundary layer winds

The vertical profile model of a downburst describes short time averaged maximum mean wind speed at a height, which may be treated as a gust profile as used in the boundary layer wind case [$V_{B-L,3-s}(z)$]. Since z_{max} and V_{max} in the Vicroy model (3) are unknown, it is necessary to establish a criterion to relate the velocity profile in a gust-front wind and a boundary layer for design considerations. In this study, two criteria are considered: i) gust-front wind speed at 10 m height, [$V_{G-F}(10)$] is set equal to the boundary layer gust speed at 10 m [Criterion 1 : $V_{G-F}(10) = V_{B-L,3-s}(10)$]; ii) the maximum gust-front wind speed (V_{max}) is equal to gust speed at the gradient height in boundary layer winds [Criterion 2 : $V_{max} = V_B$].

$L_{3-s}(10)$] (Fig. 2). Similar profile conditions were imposed in Chen and Letchford (2004b) using Wood's profile model (Wood et al. 2001).

Consideration of terrain exposure conditions (terrain roughness)

Although the vertical profile model (3) is, in reality, an analytical/empirical model based on limited full-scale data (JAWS), it represents open terrain exposure (Oseguera and Bowles 1988; Vicroy 1991) which may be treated as exposure C in ASCE 7. Thus, it is expected that there is a certain terrain roughness effect on both z_{max} and V_{max} in the Vicroy model, i.e., these two parameters may change with exposure categories in ASCE 7 (exposure B, C and D in ASCE 7-05 and exposure A, B, C and D in ASCE 7-98), whereas the model constants b_1 and b_2 (3) are assumed to be constant irrespective of the terrain roughness. Even though this terrain roughness effect on z_{max} and V_{max} has been observed by some researchers through wind-tunnel experiments, the results have been limited to showing trends in different terrain roughnesses without any quantitative estimates. These general trends exhibited higher z_{max} (e.g., Hangan and Xu 2005) and lower V_{max} (e.g., Wood et al. 2001; Choi 2004) in a built-up terrain.

One possible way to incorporate the influence of terrain roughness on z_{max} is to assume z^* (4) is a variable based on terrain roughness, where z^* is assumed to be the gradient height (z_G) of boundary layer wind profile suggested in the ASCE 7. In addition, it may be assumed that Eq. (4) is still a valid criterion regardless of terrain roughness. Accordingly, z_{max} can be obtained from z_G for each terrain exposure condition in ASCE 7 and Eq. (4), which results in z_{max} equal to 100.58 m, 80.47 m, 60.35 m and 46.94 m corresponding to

exposures A, B, C and D used in ASCE 7-98, respectively (ASCE 7-05 eliminated exposure A); First, z_{max} of 60.35 m in exposure C may be a reasonable estimate when compared to full-scale data since z_{max} has been reported to be 50~100 m based on full-scale data, which may also be regarded as exposure C (e.g., Fujita 1985; Hjermfelt 1988). Second, aside from the accuracy of z_{max} , the variation in z_{max} according to terrain roughness agrees with some experimental results (e.g., Hangan and Xu 2005).

A recent wind tunnel experiment (1:2500 scale) suggested that the height z^* did not noticeably change for different terrain roughnesses (Hangan and Xu 2005). Accordingly, Eq. (4) may be revised to reflect changes depending on terrain roughness. Although the ratio of z_{max}/z^* is still unknown for an arbitrary terrain roughness, it may be reasonable to assume that $z^* = z_G$ which would permit evaluation of this ratio for different terrain exposures. One possible approach is to follow ASCE's exposure C-based reference, e.g., basic wind speed (V_{3-s}) defined for exposure C, which can be converted to other exposures. The relationship in Eq. (4) was observed in the JAWS data collected in a terrain roughness similar to exposure C. In this manner, the ratio of z_{max}/z^* is assumed to be 0.22 in exposure C and its variation in different terrain roughness conditions is introduced by the following relationship.

$$\frac{z_{max}}{z^*} = 0.22 \frac{z_{G,A-D}}{z_{G,C}} \quad (5)$$

where, $z_{G,A-D}$ = gradient height (z_G) at arbitrary exposure condition from A–D; $z_{G,C}$ = gradient height in exposure C, approximately equal to 274 m (900 ft) (ASCE 1998, 2005). This results in z_{max}/z^* being equal to 0.37, 0.29, 0.22 and 0.12, respectively for exposures A to D. While this development certainly needs validation in full-scale measurements, it

offers a consistent trend based on the flow characteristics in different exposures, which is certainly a desirable feature in such a model.

Similarly, V_{max} is assumed to be the velocity in exposure C, and variation in V_{max} for an arbitrary terrain exposure condition is assumed to follow the respective terrain velocity relationship to that of the boundary layer wind in exposure C. Accordingly, the two profile criteria considered in the previous chapter results in the following expressions for $V_{max,C}$:

$$\text{Criterion 1 : } V_{max,C} = \frac{V_{3-s}}{1.354 \left[e^{b_1 10/z_{max,C}} - e^{b_2 10/z_{max,C}} \right]} \quad (6a)$$

$$\text{Criterion 2 : } V_{max,C} \approx 1.42V_{3-s} \quad (6b)$$

A velocity factor (V_{fac}) is introduced to facilitate convenient conversion of $V_{max,C}$ to V_{max} in other terrain exposures. It is assumed here that V_{fac} is derived from the ratio of the boundary layer wind speed at z_{max} of an arbitrary terrain exposure to boundary layer wind speed at z_{max} in exposure C.

$$V_{fac} = \frac{\hat{b}_{A-D}}{\hat{b}_C} \cdot \left(\frac{z_{max,A-D}}{10} \right)^{\hat{\alpha}_{A-D} - \hat{\alpha}_C} \quad (7)$$

where, \hat{b} , $\hat{\alpha}$ = 3-sec gust profile constants in ASCE 7; subscript C = exposure C; subscript A-D = arbitrary exposure condition from A–D (ASCE 7-98). Similarly, one may choose exposures B–D as in ASCE 7-05. As a result, V_{max} for an arbitrary terrain exposure condition can be obtained from following equation.

$$V_{max} = V_{fac} \cdot V_{max,C} \quad (8)$$

Using these definitions of z_{max} in Eq. (5) and V_{max} in Eq. (8), the vertical profile of gust-front winds for an arbitrary terrain exposure condition can be established. Table 1 provides,

for example, V_{max} and z_{max} for different terrains assuming V_{3-s} to be 40 m/s. These results follow the trends noted in experimental observations, i.e., as terrain roughness increases, V_{max} decreases but z_{max} increases. In addition, Criterion 1 [$V_{G-F}(10) = V_{B-L,3-s}(10)$] leads to higher V_{max} than Criterion 2 [$V_{max} = V_{B-L,3-s}(10)$], which reflect the distinct feature of each profile.

It is very important to emphasize here that the models utilized in this section are for the sake of establishing an analysis framework, which can conveniently incorporate additional models as they become available.

MODELING OF GUST-FRONT FACTOR

With the exemplary success of the gust loading factor (Davenport 1967) in capturing the dynamic wind effects introduced by buffeting action of wind and its popularity in design standards and codes worldwide, the authors were motivated to formulate a framework along the lines of the gust effect formulation existing in ASCE 7 (Solari 1993a, b; Solari and Kareem 1998) that encapsulates critical features of downburst winds to capture their load effects. The ‘‘Gust-Front Factor’’ (G_{G-F}) is, therefore, introduced here for use in conjunction with the existing design codes and standards. The design wind loading in a gust-front (F_{Design}) is then expressed by

$$F_{Design} = F_{ASCE\ 7} \cdot K_{z,G-F} \cdot G_{G-F} \quad (9)$$

where $F_{ASCE\ 7}$ represents the recommendation of ASCE 7 (ASCE 1998, 2005), the G_{G-F} is the gust-front factor that relates F_{Design} in a gust-front to the $F_{ASCE\ 7}$ recommendations in

conventional boundary layer winds and $K_{z,G-F}$ accounts for the velocity/pressure profile in a gust-front as opposed to boundary layer winds in ASCE 7.

The gust loading factor has been based on the displacement relationship, i.e., the ratio of the maximum displacement over mean displacement of a structure subject to wind load (Davenport 1967). Although alternative and improved formats are available, e.g., Zhou and Kareem (2001) and Chen and Kareem (2004), it was decided to conform to the current ASCE 7-05 recommendation in this study. Adaptation to other formats is convenient and immediate. Conventional gust loading factor (G_{GLF}), under the assumption of stationary winds, is defined as

$$G_{GLF} = \frac{\hat{x}_{B-L}(z, t)}{\bar{x}_{B-L}(z)} \quad (10)$$

where, subscript $B-L$ = boundary layer wind; $x_{B-L}(z, t)$ = displacement; superscripts $\hat{}$ and $\bar{}$ represent expected maximum and mean values, respectively.

As alluded to earlier, in contrast with the boundary layer winds, the gust-front winds are nonstationary due to their transient characteristics. Therefore, the stationary wind model typically used in boundary layer winds may not be valid for gust-front winds which may be described in terms of time-varying parameters. Thus, a nonstationary wind model has been introduced and given below (e.g., Wang and Kareem 2004):

$$U_{G-F}(z, t) = V_{G-F}(z, t) + u_{G-F}(z, t) \quad (11)$$

where, subscript $G-F$ = abbreviation for gust-front wind; $U_{G-F}(z, t)$ = nonstationary or time-varying gust-front wind; $V_{G-F}(t)$ = time-varying mean component of gust-front wind; $u_{G-F}(z, t)$ = fluctuating component of gust-front wind.

Several studies have pointed out that downbursts move forward with the storm-translation speed (V_{s-m}). For example, Holmes and Oliver (2000) estimated storm-translation speed from full-scale data and established an analytical downburst model for the horizontal wind speed. The storm-translation speed has been generally assumed to be 10~20 m/s by several researchers (e.g., Holmes and Oliver 2000; Savory et al. 2001; Chen and Letchford 2004a; Chay et al. 2006) and it was also employed in a recent wind-tunnel experiment (Letchford and Chay 2002). However, the time function used in this study is a half-sine pulse (2) and as such does not include storm-translation speed.

Alternatively, it may be possible to assume that the storm-translation speed is constant during a gust-front wind event and its spatial distribution with height is uniform as well, then the response due to storm movement is constant. Accordingly, the nonstationary wind model (11) is recast that includes storm-translation speed (V_{s-m})

$$U_{G-F}(z, t) = V_{G-F}(z, t) + u_{G-F}(z, t) + V_{s-m} \quad (12)$$

Therefore, the structural displacement due to gust-front winds can also be described as a nonstationary model

$$x_{G-F}(z, t) = \bar{x}_{G-F}(z, t) + \tilde{x}_{G-F}(z, t) + x_{s-m} \quad (13)$$

where, $x_{G-F}(z, t)$ = displacement under gust-front winds; $\bar{x}_{G-F}(z, t)$ = displacement due to time-varying mean component of the gust-front winds; $\tilde{x}_{G-F}(z, t)$ = displacement due to fluctuating component of gust-front winds; x_{s-m} = displacement introduced by the storm-translation speed. The corresponding maximum displacement can be expressed by

$$\begin{aligned}
\max[x_{G-F}(z,t)] &= \max[\bar{x}_{G-F}(z,t)] + \max[\tilde{x}_{G-F}(z,t)] + \max[x_{s-m}] \\
&= \max[\bar{x}_{G-F}(z,t)] \left[1 + \frac{\max[\tilde{x}_{G-F}(z,t)]}{\max[\bar{x}_{G-F}(z,t)]} + \frac{x_{s-m}}{\max[\bar{x}_{G-F}(z,t)]} \right]
\end{aligned} \tag{14}$$

The $\max[\bar{x}_{G-F}(z,t)]$ term can be rewritten as a static displacement, $\bar{x}_{st,G-F}(z)$. The time-varying mean component still contains dynamic features and therefore, unlike the mean displacement in boundary layer wind, it is recast as

$$\max[\bar{x}_{G-F}(z,t)] = \bar{x}_{st,G-F}(z) \cdot \frac{\max[\bar{x}_{G-F}(z,t)]}{\bar{x}_{st,G-F}(z)} \tag{15}$$

As mentioned earlier, the gust-front factor (G_{G-F}) as well as $K_{z,G-F}$ in Eq. (9) describes the relationship between F_{Design} in gust-front winds and F_{ASCE7} . In this study, akin to the gust loading factor (G_{GLF}) concept (10), the G_{G-F} is defined as a ratio of maximum displacements respectively in the gust-front and boundary layer winds. By using Eqs. (14) and (15), the G_{G-F} in Eq. (9) can be rewritten as

$$\begin{aligned}
G_{G-F} &= \frac{\max[x_{G-F}(z,t)]}{\max[x_{B-L}(z,t)]} \\
&= \frac{\bar{x}_{st,G-F}(z) \cdot \frac{\max[\bar{x}_{G-F}(z,t)]}{\bar{x}_{st,G-F}(z)} \cdot \left[1 + \frac{\max[\tilde{x}_{G-F}(z,t)]}{\max[\bar{x}_{G-F}(z,t)]} + \frac{x_{s-m}}{\max[\bar{x}_{G-F}(z,t)]} \right]}{\bar{x}_{B-L}(z) \cdot G_{GLF}}
\end{aligned} \tag{16}$$

It is very plausible that due to changing aerodynamics in gust-front winds the aerodynamic drag coefficient (C_D) may deviate from generally accepted C_D values due to transient characteristics of the flow around structures. The transient drag force coefficient is expressed as $C_{D,G-F}$. In order to delineate the influence of $C_{D,G-F}$ on the G_{G-F} , Eq. (16) is recast in which the drag coefficient in gust-front and boundary layer winds is separated by redefining response x as y , where the latter is response due to a unit drag force coefficient

$$G_{G-F} = \frac{\bar{y}_{st,G-F}(z)}{\bar{y}_{B-L}(z)} \cdot \frac{\max[\bar{y}_{G-F}(z,t)]}{\bar{y}_{st,G-F}(z)} \cdot \frac{\left[1 + \frac{\max[\tilde{y}_{G-F}(z,t)]}{\max[\bar{y}_{G-F}(z,t)]} + \frac{y_{s-m}}{\max[\bar{y}_{G-F}(z,t)]}\right]}{G_{GLF}} \cdot \frac{C_{D,G-F}}{C_D} \quad (17)$$

The G_{G-F} can be best captured in terms of four underlying factors, e.g., Kwon and Kareem 2007,

$$G_{G-F} = I_1 \cdot I_2 \cdot I_3 \cdot I_4 \quad (18)$$

where,

$$I_1 = \frac{\bar{y}_{st,G-F}(z)}{\bar{y}_{B-L}(z)}; \quad I_2 = \frac{\max[\bar{y}_{G-F}(z,t)]}{\bar{y}_{st,G-F}(z)}; \quad I_3 = \frac{\left[1 + \frac{\max[\tilde{y}_{G-F}(z,t)]}{\max[\bar{y}_{G-F}(z,t)]} + \frac{y_{s-m}}{\max[\bar{y}_{G-F}(z,t)]}\right]}{G_{GLF}}; \quad I_4 = \frac{C_{D,G-F}}{C_D} \quad (19)$$

In this format, the G_{G-F} takes into account the following features: variation in the vertical profile of wind speed – kinematic effects factor (mean load effects), I_1 ; dynamic effects introduced by the sudden rise in wind speed - pulse dynamics factor (rise-time effects), I_2 ; nonstationarity of turbulence in gust-front winds - structural dynamics factor (nonstationary turbulence effects), I_3 ; transient aerodynamics – potential load modification factor (transient aerodynamics effects), I_4 . Accordingly, the G_{G-F} embodies an intuitive picture of the underlying mechanisms that represent the fundamental building blocks of both the kinematic (I_1) and dynamic (I_2, I_3, I_4) load effects associated with gust-front winds on structures, distinguishing them from those experienced in conventional boundary layer flows. A schematic diagram that portrays the genesis of the design wind loads in gust-fronts is given in Fig. 3.

In the following, details of I_1 , I_2 , I_3 , I_4 and $K_{z,G-F}$ are presented. This involves a few assumptions since modeling the characteristics of gust-front winds is a subject of current research and a general consensus on the quantitative description of several items involved is still evolving. For this study the structure is limited to a building or a tower/mast structure that essentially experiences motion in the first linear mode even though the formulation can be conveniently extended to include higher order & nonlinear modes. A similar description for transmission line type structures or bridges is immediate. The mass (m), width (B) and depth (D) of the structure are assumed to be constant with height similar to the ASCE 7 design procedure that is limited to regular shaped structures with no unusual geometrical irregularities in their profile. In addition, both design loads, i.e., equivalent static wind loads (ESWL), in gust-front winds and boundary layer winds are assumed to include the wind directionality factor $K_d = 0.85$ and importance factor I (to be selected from ASCE 7-05) but no provision for topographic factor is included (i.e., $K_{zt} = 1$). Finally, the gust-front factor approach like gust loading factor is restricted to the alongwind load effects due to the buffeting action in a gust-front.

I_1 : Kinematic effects factor (mean load effects)

Factor I_1 describes mean load effects on building structure in terms of the difference between the vertical profiles in gust-front and boundary layer winds. The expression for I_1 as given in Eq. (19) can be recast as (details in Appendix I)

$$I_1 = \frac{\int_0^H V_{G-F}^2(z) \phi_1(z) dz}{\int_0^H (1/G_q) V_{B-L,3-s}^2(z) \phi_1(z) dz} \quad (20)$$

where, $V_{G-F}^2(z)$ = velocity pressure profile in gust-front winds, which is a square of the Vicroy velocity profile model (3); $\phi_l(z)$ = the linear mode shape of building ($= z/H$); G_q = gust pressure factor (A2); $V_{B-L,3-s}^2(z)$ = 3-sec gust pressure profile in ASCE 7. Following the procedure of Appendix I, Eq. (20) is approximately described as

$$I_1 \approx 1.824 \cdot G_q \cdot J_0 \cdot (\hat{\alpha} + 1) \cdot \left(\frac{z_G}{H} \right)^{2\hat{\alpha}} \cdot \left(\frac{V_{\max}}{V_{3-s}} \right)^2 \quad (21)$$

where, J_0 = weighted squared gust-front wind velocity profile with respect to linear mode shape given in Eq. (A6); H = building height; $\hat{\alpha}$ = 3-sec gust speed power law exponent in ASCE 7. In this manner, the I_l factor becomes a function of building height in a given terrain exposure.

I_2 : Pulse dynamics factor (rise-time effects)

Factor I_2 accounts for the rise-time effects during the rapid change of wind speed which is manifested as a finite duration pulse type effect and it does not include the buffeting action of turbulence which is included in the nonstationary turbulence effects (I_3). Accordingly, the time function of the gust-front wind plays an important role in the quantification of this factor.

The pulse dynamics factor (I_2) as defined in Eq. (19) can be expressed as

$$I_2 = \frac{\left[\frac{1}{M_1} \cdot \frac{1}{2} \rho B \int_0^H V_{G-F}^2(z) \phi_1(z) dz \right] \times \left[\text{max. displacement by } V_{G-F}^2(t) \right]}{\frac{1}{K_1} \cdot \frac{1}{2} \rho B \int_0^H V_{G-F}^2(z) \phi_1(z) dz} \quad (22)$$

$$= \omega_1^2 \cdot \max[x(t)]$$

where, M_1 = modal mass in the first mode, K_1 = modal stiffness in the first mode ($M_1\omega_1^2$); ω_1 = fundamental natural circular frequency ($\omega_1 = 2\pi n_1$); n_1 = fundamental natural frequency of building (Hz); $x(t)$ = building modal response to the impulsive action of the time function, $V_{G-F}^2(t)$. The solution can be obtained either by a numerical scheme, e.g., Newmark- β , or an analytical solution can be obtained using Duhamel's integral. Based on at-rest initial conditions, i.e., $x(0) = \dot{x}(0) = 0$, the analysis subject to a pulse-type loading is typically conducted in two parts, i.e., forced vibration when $t \leq t_d$ and free vibration phase when $t \geq t_d$, where t_d is pulse duration in Eq. (2). The closed-form solution and its validation are omitted here for the sake of brevity and details can be found in (Kwon and Kareem 2006a).

It is worth noting that the factor I_2 is independent of the profile shape of the gust-front wind since the profile terms are present both in the numerator and denominator and therefore are eliminated (21), thus I_2 is determined by the time function alone characterized by the pulse duration (t_d) and the building's natural frequency and damping ratio. If I_2 is larger than unity, it suggests that there exists an overshoot in response due to transient effects. In addition, I_2 always yields the same result when it is expressed in terms of the ratio of the pulse duration (t_d) and the natural period ($T_1 = 1/n_1$) (Table 2), which implies that the factor I_2 is indeed a function of the ratio of pulse duration to the natural period (t_d/T_1) as noted in most vibration textbooks. The transient effects are predominant up to $t_d/T_1 = 2$, and the pulse dynamics factor I_2 approaches unity when the pulse duration (t_d) exceeds the natural period (T_1). The maximum value of I_2 occurs when t_d is equal to the natural period ($t_d/T_1=1$).

I_3 : Structural dynamics factor (nonstationary turbulence effects)

Factor I_3 mainly accounts for nonstationary buffeting effects of turbulence in gust-front winds which are caused by the fluctuating longitudinal wind component, i.e., the component of gust-front winds with time-varying mean removed. Although the time domain approach may be the most appropriate approach to identify these effects (e.g., Chen and Letchford 2004a, b; Chay and Albermani 2005), it requires simulation of the nonstationary spatio-temporal fluctuations in wind, which demands significant additional effort. Alternatively, for linear dynamic analysis under random loading, the frequency domain approach has gained wide range acceptance as it becomes possible to formulate a closed-form solution analytically, e.g., the gust loading factor/gust effect factor approach used in ASCE 7 (e.g., Davenport 1967; Solari 1993a, b; Solari and Kareem 1998; Zhou and Kareem 2001; Zhou et al. 2002; Kareem and Zhou 2003). Extensions to nonstationary excitation have been reported in the literature (e.g., Caughey and Stumpf 1961; Barnoski and Maurer 1969; Bucciarelli and Kuo 1970; Howell and Lin 1971; Corotis et al. 1972; Hasselman 1972; Holman and Hart 1974; Corotis and Marshall 1977; Solomos and Spanos 1984; Sun and Kareem 1989; Michaelov et al. 1999a, b and 2001; Jangid 2004)

In this study for expedience, the frequency domain approach is utilized to capture wind effects due to nonstationary fluctuations in wind (Appendix II). The expected peak of the nonstationary fluctuating displacement (17, 19) is expressed in terms of the product of a peak factor and the maximum of nonstationary root-mean-square (RMS) fluctuating displacement (e.g., Sun and Kareem 1989):

$$\max[\tilde{y}_{G-F}(z,t)] = g_{G-F} \cdot \max[\sigma_{\tilde{y}_{G-F}}(t)] \quad (23)$$

where, $\tilde{y}_{G-F}(z,t)$ = displacement due to fluctuating component of gust-front winds (e.g., 13); g_{G-F} = mean peak factor (Appendix III); $\sigma_{\tilde{y}_{G-F}}(t)$ = nonstationary RMS fluctuating displacement (Appendix II). In accordance with this format, the structural dynamic factor I_3 in Eq. (19) can be recast in the following form:

$$I_3 = \frac{\left[1 + g_{G-F} \frac{\max[\sigma_{\tilde{y}_{G-F}}(t)]}{\bar{y}_{st,G-F}(z)} \cdot I_2 + I_{s-m} \right]}{G_{GLF}} \quad (24)$$

where, $\bar{y}_{st,G-F}(z)$ = static displacement of $\max[\bar{y}_{G-F}(z,t)]$ (e.g., 15); I_2 = pulse dynamics factor (19, 22); I_{s-m} = storm-translation effect factor (Appendix IV); other terms have been defined earlier.

I_4 : load modification factor (transient aerodynamics effects)

The subject of aerodynamics has been treated traditionally by invoking the quasi-steady and strip theories and has been extended to unsteady aerodynamics theories for loads originating from wake-induced effects. The current challenge is to address any quantifiable modification to aerodynamics in a transient flow environment. Earlier and more recent studies in fluid dynamics have pointed out an overshoot in aerodynamic/hydrodynamic loads on cylinders in unsteady flows (e.g., Sarpakaya 1963; Okajima 1997). In the field of aerospace engineering, such strong nonstationarity characteristics have been of concern, especially when a flight vehicle penetrates a low-altitude turbulence field over rough terrain (e.g., Howell and Lin 1971). It has also been noted that for the analysis of structures in

nonstationary atmospheric turbulence, the traditional stationary analysis fails to account for possible transient overloads, e.g., sharp changes in gusts were found to cause a transient aerodynamic force on a bridge model, which cannot be explained by conventional stationary statistical analysis (Kitigawa et al. 1982). The exposure of trains/trucks suddenly emerging from a tunnel to the energies of gust-fronts can lead to drastic aerodynamic modifications, i.e., a reversal in the sign of aerodynamic force with a change in incident flow angle, which have led to serious concerns for their operational safety. As another example, a recent study concerning pressure distributions on a wall exposed to periodic waves, large overshoots in pressure were noted due to slamming of waves on the wall (Yalla and Kareem 1999). This trend is further reaffirmed in recent experiments involving a simulated downburst utilizing a translating wall jet, which suggested that the surface pressures over a cube exceeded the quasi-steady estimates (Chay and Letchford 2002). In addition, recent study of drag forces on several two dimensional rectangular models due to sudden increase of wind velocity suggested that they showed 18 % to 25 % increase over the quasi-steady level in short time duration (Matsumoto et al. 2007). This clearly points at the need to critically assess the impact of abrupt changes in the wind field magnitudes and associated modifications in aerodynamics of structures and calls for possible refinement in the current description of load (Kareem et al. 2006; Haan 2008).

A bench top transient flow field simulator (TFFS) to generate sudden changes in wind speed that mimics gust-fronts utilizing a battery of low inertia, AC servomotor driven and individually computer-controlled fans in an open circuit wind tunnel-type test section with tailored transient flow features has been developed (Kareem et al. 2006; Butler and Kareem 2007). Similar efforts are in progress at a larger facility at Miyazaki university wind tunnel

with 99 individually controlled fans (Cao et al. 2002). In addition, efforts to explore these issues in transient aerodynamics are in place currently at several research establishments worldwide (e.g., Savory et al. 2001; Chay and Letchford 2002; McConville et al. 2007; Haan 2008; Hangan et al. 2008). In lieu of the nascent stage of developments in the transient aerodynamic effects, factor I_4 may be assumed to be unity, which implies no significant modifications to aerodynamics in transient flows. However, if current studies yield quantifiable modifications in aerodynamics, I_4 can be concomitantly adjusted.

$K_{z,G-F}$: Velocity pressure coefficient (kinematic effects)

The gust-front factor (G_{G-F}) (9) describes the relationship between F_{Design} and $F_{ASCE 7}$ concerning gust-front wind effects on building structures, which is derived by defining it as the ratio of the maximum displacements in gust-front to boundary layer winds (16). As such, the G_{G-F} definition (17, 18) lends itself to a single constant value akin to the traditional gust loading factor/gust effect factor. Thus, the constant factor may misrepresent design loads in gust-front winds (F_{Design}) as it would follow the profile of ASCE 7 even though the gust-front wind velocity/pressure profile is quite a different from the typical boundary layer wind profile (e.g., Fig. 2a, b).

To account for this profile issue in the gust-front factor approach, a ‘velocity pressure coefficient’ denoted by $K_{z,G-F}$ is introduced here. In the ASCE 7 procedure, the design load ($F_{ASCE 7}$) is proportional to the velocity pressure exposure coefficient (K_z) which is square of the velocity in boundary layer winds (A3); details can be found in Appendix I. Thus, design load variations along the height in gust-front winds (F_{Design}) should be proportional to the

square of the gust-front wind velocity at its respective elevation in the velocity profile, i.e., $V_{G-F}^2(z)$ (3). In this manner, $K_{z,G-F}$ will be the ratio of the square of velocity in the respective profiles, i.e., gust-front and boundary layer winds.

Since velocity pressure profiles in F_{Design} and F_{ASCE7} are different and height-dependent, a concept similar to generalized mass in modal coordinates is utilized to normalize velocity pressure profile. Accordingly, $K_{z,G-F}$ is expressed as a ratio of normalized velocity pressure profiles in gust-front and boundary layer winds:

$$K_{z,G-F} = \frac{V_{G-F}^2(z)\phi_1(z) / \int_0^H V_{G-F}^2(z)\phi_1(z)dz}{(1/G_q)V_{B-L,3-s}^2(z)\phi_1(z) / \int_0^H (1/G_q)V_{B-L,3-s}^2(z)\phi_1(z)dz} \quad (25)$$

In terms of factor I_1 (20), Eq. (25) can be recast as

$$K_{z,G-F} = \frac{1}{I_1} \cdot \frac{V_{G-F}^2(z)}{(1/G_q)V_{B-L,3-s}^2(z)} \quad (26)$$

Accordingly, $K_{z,G-F}$ also belongs to the category of kinematic effects in I_1 , since it involves the distribution of velocity/pressure in both flows.

It is worth noting that for conventional boundary layer winds, both the gust-front factor (G_{G-F}) and the velocity pressure coefficient ($K_{z,G-F}$) in gust-front winds reduce to unity. Therefore, the conventional gust loading/effect factor approach in ASCE 7 becomes a special case of the proposed gust-front factor approach. It is also noted that due to the nose-shape profile of gust-fronts (e.g., Fig. 2a, b), ‘local loading effect’, e.g., interstory drift for cladding may become more prominent. Depending on building properties and characteristics of gust-front winds in the design procedure, it is necessary to adjust F_{Design} in

the final design stage to select the maximum equivalent static load due to either a gust-front condition or boundary layer winds as each may control at different heights due to the nature of their respective profiles (Fig. 4). The final distribution is referred to as F_{Final} here.

PARAMETRIC STUDY ON GUST-FRONT FACTOR

Three example buildings are considered to evaluate and demonstrate the application of the gust-front factor (G_{G-F}). The following features are common for these examples: building density $\rho_B = 180 \text{ kg/m}^3$, air density $\rho_a = 1.225 \text{ kg/m}^3$ (ASCE 7), damping ratio $\zeta_1 = 0.01$, basic wind speed $V_{3-s} = 40 \text{ m/s}$, pulse durations $t_d = 5, 10, 100, 200 \text{ sec}$, terrain exposure conditions – exposure B and C; storm-translation speed $V_{s-m} = 12 \text{ m/s}$; I_4 is assumed to be unity in this study. Building dimensions and natural frequencies are: 1) $B = D = 20 \text{ m}$, $H = 60 \text{ m}$, $n_1 = 0.8 \text{ Hz}$ ($T_1 = 1.25 \text{ sec}$); 2) $B = D = 20 \text{ m}$, $H = 100 \text{ m}$, $n_1 = 0.4 \text{ Hz}$ ($T_1 = 2.5 \text{ sec}$); 3) $B = D = 40 \text{ m}$, $H = 200 \text{ m}$, $n_1 = 0.2 \text{ Hz}$ ($T_1 = 5 \text{ sec}$).

Table 3 and 4 show the results for exposure B and C, respectively. Overall, I_2 has values larger for short pulse durations due to the transient dynamic effects. For example, $t_d = 5 \text{ sec}$ in building 3 has the largest I_2 value since the pulse duration (t_d) is close to building natural period T_1 of 5 sec ($1 / 0.2 \text{ Hz}$) as given in Table 2. Factor I_3 generally increases as pulse duration t_d increases, except for $t_d = 10 \text{ sec}$ in building 3, where transient dynamic effects are dominant. In most cases, factor I_3 turns out to be less than unity implying that the nonstationary turbulence effects of gust-front winds may not be significant in those cases due to the short duration of the event, i.e., the peak response may not have the time to attain values comparable to those in stationary cases. A similar observation was made in

Chay and Albermani (2005) in terms of a time domain dynamic analysis based on simulated nonstationary winds. It is noted that a product of I_2 , I_3 and I_4 less than unity suggests that the total dynamic effects in the modeled gust-front winds are less significant than those in conventional boundary layer winds. The kinematic effects factor I_1 shows quite a marked difference between the two Criteria implying that Criterion 1 has larger profile effect than that of Criterion 2, which reflects the distinct feature of each profile criterion (Table 1).

Based on the gust-front factor approach, the design loads (ESWL) that include F_{ASCE7} and F_{Final} for the three buildings in the case of $t_d = 200$ sec are shown in Fig. 5. It is obvious that Criterion 1 (Figs. 5a, b) is more critical than Criterion 2 (Figs. 5c, d) since V_{max} in Criterion 1 is always larger than Criterion 2 regardless of the terrain exposure. In addition, since the ESWL in gust-front winds are proportional to the square of wind velocity profile ($V_{G-F}^2(z)$), which exhibits higher z_{max} and lower V_{max} in a built-up terrain (Table 1), the distribution of ESWL along the height therefore, reflects the same trend (Fig. 5). Despite the relatively lower significance of the dynamic effects contributed by the pulse dynamics (I_2) and nonstationary turbulence (I_3) aspects (Tables 3 and 4), the kinematic effects due to the wind profile (I_1 and $K_{z,G-F}$) result in locally enhanced loads around z_{max} , therefore, buildings 1 and 2 show higher load enhancements than building 3 (Fig. 5). This underscores the role of enhancement in the kinematic effects introduced through factor I_1 and the velocity pressure coefficient ($K_{z,G-F}$) to the overall design load even though the dynamic effects (I_2 and I_3) were not significant for these particular examples. One should not overlook the possible load enhancement due to transient aerodynamics, which may be

attributed to the changes in the aerodynamics associated with the fast moving front around the building with better spatial correlation of the flow field. This factor may result in enhancing local pressures or overall force coefficient in the neighborhood of 5–20 % based on preliminary observations thus far (e.g., Butler and Kareem 2007; Matsumoto et al. 2007).

A FRAMEWORK FOR WEB-BASED ON-LINE GUST-FRONT FACTOR

The introduction of the gust-front factor approach for estimating design loads in gust-front wind offers a comprehensive genesis of mechanisms involved. However, its inclusion in a standard as such may become a source of additional computational burden on a design engineer. This is particularly relevant in light of criticism over the current gust effect factor formulation and the attendant calculation procedure from some circles of ASCE 7-05 users.

In view of the complexity of the problem, a web-based portal to assess the design loads in gust-front winds in an e-design format is introduced to facilitate and promote the usage of the gust-front factor approach. This would also permit on-the-fly evaluation of a number of loading cases which otherwise would require extensive calculation. This gust-front factor approach is the first step towards quantifying gust-front wind load effects on buildings with several assumptions, e.g., vertical profile of gust-front winds and their relationship to boundary layer winds. Nonetheless, it offers a fundamental framework that can be used at this stage and continually improved as additional information becomes available.

This web-based on-line gust-front factor framework has a user-friendly interface shown in Fig. 6, and is available at <http://gff.ce.nd.edu>. Along with two profile criteria, this portal offers a user-defined gust-front wind profile, i.e., V_{max} and z_{max} based on Vicroy model (3).

Thus, the user can not only utilize the two profile criteria defined in this study, but also any arbitrary V_{max} and z_{max} inputs for the on-line determination of gust-front wind load effects on buildings, i.e., gust-front factor and corresponding design loads (ESWL). Once the input is completed, the following quantities are then displayed in the results interface (Fig. 7): input parameters selected by the user to confirm user inputs; kinematic effects factor (mean load effect factor, I_1); dynamic effects factors (I_2 , I_3 and I_4); gust-front factor (G_{G-F}); a figure that displays the ESWL in ASCE 7 (F_{ASCE7}), the ESWL in gust-front wind (F_{Design}) and the F_{Final} which selects larger load from F_{ASCE7} and F_{Design} at each story level.

One added feature in this gust-front factor portal is that it also includes the ASCE 7-98 (for exposure A) and 7-05 procedure for boundary layer winds which is available by selecting this option in the user-interface (Fig. 6). This procedure does not include the topographic factor (i.e., $K_{zt} = 1$), the wind directionality factor (K_d) of 0.85 is used and only loading for the main force resisting systems is provided. The output of ASCE 7-05 procedure are the gust loading factor/gust effect factor and the ESWL (F_{ASCE7}), maximum alongwind displacement, the RMS and peak alongwind accelerations as a function of height above the ground surface. An example in the ASCE 7-05 (Table C6-9) is utilized to validate this on-line feature though not cataloged here for brevity (Kwon and Kareem 2006c).

CONCLUDING REMARKS

Consideration of winds associated with gust-fronts, underscored by the frequency of observed damage due to these winds, has emerged as a critical issue in the field of

wind/structural engineering. Design wind loads based on conventional analysis frameworks in codes and standards may not accurately describe this fundamentally different wind event that departs from typical boundary layer winds both in its kinematics and dynamics. This paper proposes a gust-front factor approach that systematically accounts for the changes in load effects in gust-front winds and can be used in conjunction with the existing design standards. The conventional gust loading factor/gust effect factor approach in ASCE 7 becomes a special case of the proposed scheme as the gust-front factor (G_{G-F}) and velocity pressure coefficient ($K_{z,G-F}$) reduce to unity. In the examples studied here, it is observed that as a result of gust-fronts winds, a higher local ESWL distribution exists despite the fact that the dynamic effects ($I_2 \cdot I_3 \cdot I_4$) for these buildings were less than unity. This highlights the role of enhancement in the kinematic effects introduced through the kinematic effect factor (I_1) and velocity pressure coefficient ($K_{z,G-F}$) to the overall design load even though the dynamic effects are not prevalent in these examples. The proposed gust-front factor based analysis framework lays the foundation for the analysis of structures under gust-front winds, which is akin to the gust loading factor/gust effect factor in conventional winds. It can be conveniently tailored for design standards other than ASCE 7. It is anticipated that it would experience further refinements over time similar to the many subsequent developments in the original procedure of conventional gust loading factor. For immediate design applications, this framework is available in a user-friendly web-based portal (<http://gff.ce.nd.edu>) which will offer the flexibility of examining several loading configurations on-the-fly without actually becoming involved with the details of the

computations. This feature promises to make this design procedure very attractive regardless of the user's background in the various underlying computations.

ACKNOWLEDGEMENTS

The authors are grateful for the financial support provided by NSF Grant CMMI 03-24331. The authors also wish to acknowledge Ms. Rachel Bashor and Mr. Kyle Butler, NatHaz Modeling Laboratory, University of Notre Dame for their input during the development of this procedure.

NATHAZ Modeling Laboratory
University of Notre Dame

REFERENCES

- Alahyari, A., and Longmire, E. K. (1995). "Dynamics of experimentally simulated microburst." *AIAA Journal*, 33(11), 2128-2136.
- American Society of Civil Engineers (ASCE) (1998). *Minimum design loads for buildings and other structures*, ASCE 7-98, ASCE, Reston, VA.
- American Society of Civil Engineers (ASCE) (2005). *Minimum design loads for buildings and other structures*, ASCE 7-05, ASCE, Reston, VA.
- Barnoski, R. L., and Maurer, J. R. (1969). "Mean-square response of simple mechanical systems to nonstationary random excitation." *J. App. Mech.*, ASME, 36(2), 221-227.
- Bucciarelli, L. L., Jr., and Kuo, C. (1970). "Mean-square response of a second-order system to nonstationary random excitation." *J. App. Mech.*, ASME, 37(3), 612-616.
- Butler, K., and Kareem, A. (2007). "Physical and numerical modeling of downburst generated gust fronts." *Proc. 12th International Conference on Wind Engineering*, Cairns, Australia, 791-798.
- Cao, S., Nishi, A., and Kikugawa, H. (2002). "Reproduction of wind velocity history in a multiple fan wind tunnel." *J. Wind. Eng. Ind. Aerodyn.*, 90, 1719-1729.
- Caughey, T. K., and Stumpf, H. J. (1961). "Transient response of a dynamic system under random excitation." *J. App. Mech.*, ASME, 28(4), 563-566.
- Chay, M. T., and Letchford, C. W. (2002). "Pressure distributions on a cube in a simulated thunderstorm downburst. Part A : stationary downburst observations." *J. Wind. Eng. Ind. Aerodyn.*, 90(7), 711-732.

- Chay, M., and Albermani, F. (2005). "Dynamic response of a SDOF system subjected to simulated downburst winds." *Proc. of the Sixth Asia-Pacific Conference on Wind Engineering (APCWE-VI)*, Seoul, Korea, 1562-1584.
- Chay, M., Albermani, F., and Wilson, R. (2006). "Numerical and analytical simulation of downburst wind loads." *Eng. Struct.*, 28(2), 240-254.
- Chen, X. and Kareem, A. (2004). "Equivalent static wind loads on buildings: A new model", *J. Struct. Eng.*, ASCE, 130(10), 1425-1435.
- Chen, L., and Letchford, C. W. (2004a). "A deterministic-stochastic hybrid model of downbursts and its impact on a cantilevered structure." *Eng. Struct.*, 26(5), 619-629.
- Chen, L., and Letchford, C. W. (2004b). "Parametric study on the along-wind response of the CAARC building to downbursts in the time domain." *J. Wind. Eng. Ind. Aerodyn.*, 92(9), 703-724.
- Chen, L., and Letchford, C. W. (2005a). "A Nonparametric Deterministic-Stochastic Hybrid Model for Nonstationary Wind Speeds." *Proc. 10th Americas Conference on Wind Engineering* (CD-ROM), Baton Rouge, LA, Paper No. 063, AAWE.
- Chen, L., and Letchford, C. W. (2005b). "Simulation of extreme winds from thunderstorm downbursts." *Proc. 10th Americas Conference on Wind Engineering* (CD-ROM), Baton Rouge, LA, Paper No. 064, AAWE.
- Chen, L., and Letchford, C. W. (2006). "Multi-scale correlation analyses of two lateral profiles of full-scale downburst wind speeds." *J. Wind. Eng. Ind. Aerodyn.*, 94(9), 675-696.
- Choi, E. C. C., and Hidayat, F. A. (2002). "Dynamic response of structures to thunderstorm winds." *Progress in Structural Engineering and Materials*, 4(4), 408-416.

- Choi, E. C. C. (2004). "Field measurement and experimental study of wind speed profile during thunderstorms." *J. Wind. Eng. Ind. Aerodyn.*, 92(3-4), 275-290.
- Corotis, R. B., Vanmarcke, E. H., and Cornell, C. A. (1972). "First passage of nonstationary random processes." *J. Eng. Mech. Div.*, ASCE, 98(EM2), 401-414.
- Corotis, R. B., and Marshall, T. A. (1977). "Oscillator response to modulated random excitation." *J. Eng. Mech. Div.*, ASCE, 103(EM4), 501-513.
- Davenport, A. G. (1964). "Note on the distribution of the largest value of a random function with application to gust loading." *Proc. Institution of Civil Engineers*, 28, 187-196.
- Davenport, A. G. (1967). "Gust loading factors." *J. Struct. Div.*, ASCE, 93(3), 11-34.
- Fujita, T. T. (1985). *The Downburst*, SMRP Research Paper No. 210.
- Fujita, T. T. (1990). "Downbursts : Meteorological features and wind field characteristics." *J. Wind. Eng. Ind. Aerodyn.*, 36(1), 75-86.
- Gast, K. D., and Schroeder, J. L. (2003). "Supercell rear-flank downdraft as sampled in the 2002 thunderstorm outflow experiment." *Proc. 11th International Conference on Wind Engineering* (CD-ROM), Lubbock, TX, Paper No. C08-2.
- Haan, F. L. (2008). "Simulation of non-stationary extreme wind events." *Proc. 3rd International Symposium on Wind Effects on Buildings and Urban Environment* (CD-ROM), Tokyo, Japan.
- Hangan, H., Roberts, D., Xu, Z., and Kim, J-D. (2003). "Downburst simulations. Experimental and numerical challenges." *Proc. 11th International Conference on Wind Engineering* (CD-ROM), Lubbock, TX, Paper No. C08-3.

- Hangan, H., and Xu, Z. (2005). "Scale and roughness effects in impinging jets with application to downburst simulations." *Proc. 10th Americas Conference on Wind Engineering* (CD-ROM), Baton Rouge, LA, Paper No. 068, AAWE.
- Hangan, H., Hashemi-Tari, P. and Kim, J. (2008). "Modeling of High Intensity Winds." *Proc. 2008 ASCE Structures Congress* (CD-ROM), Vancouver, Canada, Paper No. 378, ASCE.
- Hasselman, T. (1972). "Linear response to nonstationary random excitation." *J. Eng. Mech. Div.*, 98(EM3), 519-530.
- Hjelmfelt M. R. (1988). "Structure and life cycle of microburst outflows observed in Colorado." *J. App. Meteo.*, 27(8), 900-927.
- Holman, R. E., and Hart, G. C. (1974). "Nonstationary response of structural systems." *J. Eng. Mech. Div.*, 100(EM2), 415-431.
- Holmes, J. D., and Oliver, S. E. (2000). "An empirical model of a downburst." *Eng. Struct.*, 22(9), 1167-1172.
- Howell, L. J., and Lin, Y. K. (1971). "Response of flight vehicles to nonstationary atmospheric turbulence." *AIAA Journal*, 9(11), 2201-2207.
- Jangid, R. S. (2004). "Response of SDOF system to non-stationary earthquake excitation." *Earthquake Engineering and Structural Dynamics*, 33(15), 1417-1428.
- Kareem, A., and Zhou, Y. (2003). "Gust loading factor – past, present and future." *J. Wind. Eng. Ind. Aerodyn.*, 91(12-15), 1301-1328.
- Kareem, A., Butler, K., and Kwon, D. (2006). "Modeling and simulation of transient wind load effects." *Proc. 4th UJNR Panel on Wind and Seismic Effects Workshop on Wind Engineering* (CD-ROM), Tsukuba, Tokyo.

- Kikitsu, H., Kanda, J., and Iwasaki, R. (1999). "Flow simulation by wind tunnel with computer-controlled multiple fans." *J. Wind. Eng. Ind. Aerodyn.*, 83, 421-429.
- Kim, J., and Hangan H. (2007). "Numerical simulations of impinging jets with application to downbursts", *J. Wind. Eng. Ind. Aerodyn.*, 95(4), 279-298
- Kitigawa, M., Shiriashi, N. and Matsumoto, M. (1982). "Fundamental study on transient properties of lift force in an unsteady flow." *Proc. 37th Annual Conference of the Japan Society of Civil Engineering*, Japan (in Japanese).
- Kwon, D., Kijewski-Correa, T., and Kareem, A. (2005). "e-Analysis/Design of tall buildings subjected to wind loads." *Proc. 10th Americas Conference on Wind Engineering* (CD-ROM), Baton Rouge, LA, Paper No. 123, AAWE.
- Kwon, D. K., and Kareem, A. (2006a). "Gust-front factor : A new framework for design loads in gust-fronts – Part A: Definition, formulation and implementation of gust-front factor.", NatHaz Modeling Laboratory Report, University of Notre Dame.
- Kwon, D. K., and Kareem, A. (2006b). "Gust-front factor : A new framework for design loads in gust-fronts – Part B: RMS response and nonstationary Turbulence Effects.", NatHaz Modeling Laboratory Report, University of Notre Dame.
- Kwon, D. K., and Kareem, A. (2006c). "Gust-front factor : A new framework for design loads in gust-fronts – Part C: Velocity pressure coefficient on design loads and web-based on-line framework.", NatHaz Modeling Laboratory Report, University of Notre Dame.

- Kwon, D., and Kareem, A. (2007). "Gust-front factor: A new framework for the analysis of wind load effects in gust-fronts." *Proc. 12th International Conference on Wind Engineering*, Cairns, Australia, 767-774.
- Letchford, C. W. and Chay, M. T. (2002). "Pressure distributions on a cube in a simulated thunderstorm downburst. Part B : moving downburst observations." *J. Wind. Eng. Ind. Aerodyn.*, 90(7), 733-753.
- Lin, W. E., and Savory E. (2006). "Large-scale quasi-steady modeling of a downburst outflow using a slot jet.", *Wind and Structures*, 9(6), 419-440.
- Mason, M. S., Wood, G. S., and Fletcher D. F. (2007). "A simple atmospheric downburst model for wind engineering application." *Proc. 12th International Conference on Wind Engineering*, Cairns, Australia, 1447-1454.
- Matsumoto, M., Shimanura, M., Maeda, T., Shirato, H., Yagi, T., Hori, K., Kawashima, Y. and Hashimoto, M. (2007). "Drag forces on 2-D cylinders due to sudden increase of wind velocity." *Proc. 12th International Conference on Wind Engineering*, Cairns, Australia, 1727-1734.
- McConville, A., Sterling, M., and Baker, C. (2007). "An introduction of the scaling issues associated with the physical simulation of thunderstorm downbursts." *Proc. 12th International Conference on Wind Engineering*, Cairns, Australia, 1431-1438.
- Michaelov, G., Sarkani, S., and Lutes, L. D. (1999a). "Spectral characteristics of nonstationary random processes – a critical review." *Structural Safety*, 21(3), 223-244.
- Michaelov, G., Sarkani, S., and Lutes, L. D. (1999b). "Spectral characteristics of nonstationary random processes – response of a simple oscillator." *Structural Safety*, 21(3), 245-267.

- Michaelov, G., Lutes, L. D., and Sarkani, S. (2001). "Extreme value of response to nonstationary excitation." *J. Eng. Mech.*, ASCE, 127(4), 352-363.
- Okajima, A., Matsumoto, T. and Kimura, S. (1997). "Force Measurements and flow visualization of bluff bodies in oscillatory flow." *J. Wind. Eng. Ind. Aerodyn.*, 69-71, 213-228.
- Oseguera, R. M., and Bowles, R. L. (1988). "A simple, analytical 3-dimensional downburst model based on boundary layer stagnation flow." *NASA Technical Memorandum*, 100632.
- Priestley, M. B. (1965). "Evolutionary spectra and non-stationary processes.", *J. Royal Statistical Society. Series B (Methodological)*, 27(2), 204-237.
- Priestley, M. B. (1967). "Power spectral analysis of nonstationary random process." *J. Sound and Vibration*, 6(1), 86-97.
- Sarpkaya, T. (1963). "Lift, drag, and mass coefficients for a circular cylinder immersed in time dependent flow." *J. App. Mech.*, ASME, 30(1), 13-15.
- Savory E., Parke, G. A. R., Zeinoddini, M., Toy, N., and Disney, P. (2001). "Modelling of tornado and microburst-induced wind loading and failure of a lattice transmission tower." *Eng. Struct.*, 23(4), 365-375.
- Simiu, E, and Scanlan, R. H. (1996). *Wind effects on structures*, Third edition, John Wiley & Sons, Inc.
- Solari, G. (1993a). "Gust buffeting. I : Peak wind velocity and equivalent pressure." *J. Struct. Eng.*, ASCE, 119(2), 365-382.
- Solari, G. (1993b). "Gust buffeting. II : Dynamic along-wind response." *J. Struct. Eng.*, ASCE, 119(2), 383-397.

- Solari, G., and Kareem, A. (1998). "On the formulation of ASCE 7-95 gust effect factor." *J. Wind. Eng. Ind. Aerodyn.*, 77-78, 673-684.
- Solomos, G. P., and Spanos, P.-T. D. (1984). "Oscillator response to nonstationary excitation." *J. Appl. Mech.*, 51(4), 907-912.
- Sun, W.-J., and Kareem, A. (1989). "Response of MDOF systems to nonstationary random excitation." *Eng. Struct.*, 11(2), 83-91.
- Vicroy, D. D. (1991). "A simple, analytical, axisymmetric microburst model for downdraft estimation." *NASA Technical Memorandum*, 104053.
- Vicroy, D. D. (1992). "Assessment of microburst models for downdraft estimation." *J. Aircraft*, AIAA, 29(6), 1043-1048.
- Wang, L., and Kareem, A. (2004). "Modeling of non-stationary winds in gust-fronts." *Proc. 9th ASCE Joint Specialty Conference on Probabilistic Mechanics and Structural Reliability* (CD-ROM), PMC2004, Albuquerque, NM.
- Wang, L., and Kareem, A. (2005). "Modeling and simulation of transient winds: Downbursts/Hurricane." *Proc. 10th Americas Conference on Wind Engineering* (CD-ROM), Baton Rouge, LA, Paper No. 097, AAWE.
- Wood, G. S., Kwok, K. C. S., Motteram, N. A., and Fletcher, D. F. (2001). "Physical and numerical modelling of thunderstorm downbursts." *J. Wind. Eng. Ind. Aerodyn.*, 89(6), 535-552.
- Xu, Y. L., and Chen, J. (2004). "Characterizing nonstationary wind speed using empirical mode decomposition." *J. Struct. Eng.*, ASCE, 130(6), 912-920.

- Xu, Z., and Hangan, H. (2005). "Analytical Models for Impinging Jets with application to Downburst Simulations." *Proc. 10th Americas Conference on Wind Engineering* (CD-ROM), Baton Rouge, LA, Paper No. 073, AAWE.
- Yao, J., and Lundgren, T. S. (1996). "Experimental investigation of microbursts." *Experiments in Fluids*, 21(1), 17-25.
- Yalla, S. K., and Kareem, A. (1999). "Modeling tuned liquid dampers as 'sloshing-slamming' dampers." *Proc. 10th International Conference on Wind Engineering*, Copenhagen, Denmark, 1569-1575.
- Zhou, Y., and Kareem, A. (2001). "Gust loading factor: New model." *J. Struct. Eng.*, ASCE, 127(2), 168-175.
- Zhou, Y., and Kijewski, T. and Kareem, A. (2002). "Along-wind load effects on tall buildings: comparative study of major international codes and standards." *J. Struct. Eng.*, ASCE, 128(6), 788-796.

APPENDIX I. FORMULATION OF KINEMATIC EFFECTS FACTOR (I_1)

Factor I_1 is defined as the ratio of the static (mean) response in gust-front and boundary layer winds and is expressed as $I_1 = \bar{y}_{st,G-F}(z) / \bar{y}_{B-L}(z)$ (19), where the static response results from the static wind velocity pressure [= $1/2\rho V^2(z)$]. By invoking a modal analysis procedure, the static response in a gust-front is expressed as

$$\bar{y}_{st,G-F}(z) = \frac{1}{K_1} \frac{1}{2} \rho_a B \int_0^H V_{G-F}^2(z) \phi_1(z) dz \cdot \phi_1(z) \quad (A1)$$

where, K_1 = modal stiffness in the first linear mode; ρ_a = air density (= 1.225 kg/m³ in ASCE 7); B = building width.

It is noted that ASCE 7 utilizes 3-sec gust speed (V_{3-s}) and profile for the calculation of static wind velocity pressure, whereas the gust loading factor is derived based on a hourly mean wind speed and profile. To compensate for this difference in averaging time, gust pressure factor (G_q) has been introduced in ASCE 7:

$$G_q = (1 + 1.7 g_v I_{\bar{z}}) \quad (A2)$$

where, g_v = peak factor taken as 3.4 (ASCE 7); $I_{\bar{z}}$ = turbulence intensity in \bar{z} ; \bar{z} = equivalent height of structure (= $0.6H$) (e.g., Solari and Kareem 1998; Zhou et al. 2002). In this manner, the static wind velocity pressure in ASCE 7 is expressed as $0.5\rho V_{B-L,3-s}^2(z) / G_q$, where $V_{B-L,3-s}^2(z)$ = velocity pressure profile based on 3-sec gust. In

ASCE 7, the velocity pressure exposure coefficient (K_z) is defined as

$$K_z = 2.01 \left(\frac{z}{z_G} \right)^{2\hat{\alpha}} \quad (A3)$$

Note that ASCE 7 utilizes the separation of pressure coefficient (C_p) into windward (C_{pw}) and leeward (C_{pl}) components and velocity pressure exposure coefficient (K_z) in boundary layer winds (A3) is defined as two height regions, i.e., $z < 4.57$ m (15 ft) and $4.57 \text{ m} \leq z \leq z_G$ (ASCE 7).

Accordingly, the static response in ASCE 7 can be expressed as

$$\bar{y}_{B-L}(z) = \frac{1}{K_1} \frac{1}{2} \rho_a B \int_0^H (1/G_q) V_{B-L,3-s}^2(z) \phi_1(z) dz \cdot \phi_1(z) \quad (\text{A4})$$

From Eqs. (A1) and (A4), factor I_1 is recast as

$$I_1 = \frac{\int_0^H V_{G-F}^2(z) \phi(z) dz}{\int_0^H (1/G_q) V_{B-L,3-s}^2(z) \phi(z) dz} = \frac{\int_0^H \left\{ 1.354 V_{\max} \left[e^{-0.22z/z_{\max}} - e^{-2.75z/z_{\max}} \right] \right\}^2 (z/H) dz}{\frac{1}{G_q} \int_0^H \frac{V_{3-s}^2 \left[C_{pw} K_z(z) - C_{pl} K_z(H) \right]}{(C_{pw} - C_{pl})} (z/H) dz} \quad (\text{A5})$$

where, $(C_{pw} - C_{pl})$ is utilized to eliminate pressure coefficient effect from being in the numerator $[C_{pw} K_z(z) - C_{pl} K_z(H)]$.

If pressure coefficient C_p is assumed as simply $(C_{pw} - C_{pl})$ and the K_z region below 4.57 m is ignored, which result in $V_{B-L,3-s}^2(z) = V_{3-s}^2 \cdot K_z(z)$, Eq. (A5) is approximated as Eq. (21), where J_0 is given below:

$$J_0 = \int_0^1 \left[e^{d_1 Z} - 2e^{d_2 Z} + e^{d_3 Z} \right] Z dZ = \left[\frac{1}{d_1^2} (d_1 e^{d_1} - e^{d_1} + 1) - \frac{2}{d_2^2} (d_2 e^{d_2} - e^{d_2} + 1) + \frac{1}{d_3^2} (d_3 e^{d_3} - e^{d_3} + 1) \right] \quad (\text{A6})$$

where, $d_1 = -0.44H/z_{\max}$; $d_2 = -2.97H/z_{\max}$; $d_3 = -5.50H/z_{\max}$.

APPENDIX II. NONSTATIONARY RMS RESPONSE

To implement and simplify the frequency domain approach to nonstationary turbulence of gust-front winds, a number of assumptions are introduced: First, nonstationary fluctuating wind is comprised of a time-varying standard deviation wind component and a normalized fluctuating wind component, and the latter is a zero mean stationary Gaussian process (e.g., Howell and Lin 1971; Chen and Letchford 2005a, b; Chay and Albermani 2005; Chay et al. 2006). Second, the nonstationary fluctuating wind is described by the evolutionary power spectrum (Priestley 1965, 1967). Third, the normalized fluctuating wind component is represented by the Davenport wind spectrum and coherence functions in the horizontal and vertical directions (Davenport 1967). It is very plausible that wind field in downbursts may be more correlated than conventional boundary layer winds which can be accommodated in this probabilistic format of multiple point formulation.

While a detailed description of the nonstationary RMS response in the frequency domain can be found in Kwon and Kareem (2006b), a brief summary is provided here.

Nonstationary fluctuating wind load spectrum in gust-front wind

The nonstationary fluctuating wind, $u_{G-F}(z,t)$ in Eq. (12) is decomposed into an amplitude modulating function and a stationary wind component:

$$u_{G-F}(z,t) = A(z,t) \cdot u_s(z,t) = c_1 \cdot V_{G-F}(t) \cdot V_{G-F}(z) \cdot u_s(z,t) \quad (\text{A7})$$

where, $A(z,t)$ = amplitude modulating function; c_1 = amplitude modulating coefficient;

$u_s(z,t)$ = normalized stationary Gaussian process of fluctuating component with a zero mean

which is obtained from the normalized Davenport wind spectrum ($S_{u,s}(n) = S_u(n)/\sigma_u^2$); $\sigma_u^2 =$

variance of fluctuating wind speed generally defined as $\sigma_u^2 = 6u_*^2$ where u_* is friction velocity (e.g., Simiu and Scanlan 1996). Note that $u_s(z,t)$ can be reduced to $u_s(t)$ due to the height-independency of Davenport wind spectrum.

In terms of this decomposition, the amplitude modulating coefficient (c_I) plays the role of constant turbulence intensity (I_z). For example, Chen and Letchford (2004a) assumed c_I as 0.25 first, then they suggested 0.08 to 0.11 in a later publication (Chen and Letchford 2006; Chay et al. 2006), while others have used a range of c_I values from 0.01 to 0.25 (Chay and Albermani 2005). However, since a single constant c_I may not be valid for arbitrary terrain exposures, this study assumes c_I as turbulence intensity at each terrain exposure which is defined in ASCE 7's turbulence intensity (I_z) expression:

$$c_I = c \left(\frac{10}{0.6H} \right)^{1/6} \quad (\text{A8})$$

where, c = constant for arbitrary terrain exposures (ASCE 7-98, 7-05). As an example of building height $H = 200$ m, c_I becomes 0.30, 0.20, 0.13 and 0.10 corresponding to exposure A, B, C and D used in ASCE 7-98.

Similar to the general frequency domain approach in boundary layer winds (e.g., Davenport 1967; Choi and Hidayat 2002; Kareem and Zhou 2003), the time-dependent fluctuating wind force spectrum of gust-front winds is expressed in terms of the evolutionary spectrum concept (Priestley 1965, 1967):

$$\begin{aligned} S_{f,G-F}(n,t) &= (\rho_a \cdot c_1)^2 \cdot S_{u,s}(n) \cdot V_{G-F}^4(t) \times \\ &\quad \int_0^H \int_0^H V_{G-F}^2(z_1) V_{G-F}^2(z_2) R_x(z_1, z_2, n) R_z(z_1, z_2, n) \phi_1(z_1) \phi_1(z_2) dz_1 dz_2 \\ &= (\rho_a \cdot c_1)^2 \cdot S_{u,s}(n) \cdot V_{G-F}^4(t) \cdot |J_{z_1}(n)|^2 \cdot |J_{x_1}(n)|^2 \end{aligned} \quad (\text{A9})$$

where, R_x, R_z = coherence functions of the horizontal and vertical directions (Davenport 1967), respectively; $|J_{x1}(n)|^2, |J_{z1}(n)|^2$ = vertical and horizontal joint acceptance functions, respectively. Owing to height-independent characteristics of the Davenport wind spectrum, the normalized spectrum $[S_{u,s}(n)]$ can be taken out of double integration (A9) which alleviates a more extensive calculation.

Since the distribution of the mean wind speed of a gust-front wind with height is still under study, $V(10)$ -based coherence functions are utilized here instead of the widely used $V(z)$ -based functions in boundary layer winds, as the Davenport wind spectrum is also based on $V(10)$ (e.g., Simiu and Scanlan 1996). This study utilizes the mean wind speed $V(10)$ in both the Davenport wind spectrum and coherence functions of gust-front winds as $0.2V_{G-F}(10)$, referring to previous studies (e.g., Chen and Letchford 2004a; Chay et al. 2006). It is known that exponential decay coefficients C_x and C_z in $V(10)$ -based coherence functions are height-dependent coefficients, however, for practical purpose, coefficient 6 in both coefficients, taking approximated mean value from height-coefficients plots shown in Simiu and Scanlan (1996), is utilized. This coefficient may lead to quite a high correlation with height, however, it is expected that gust-front winds may have higher correlation with height than typical boundary layer winds due to the characteristics of relatively short time event.

Time-dependent transfer function

In the frequency domain approach, root-mean-square (RMS) response in boundary layer winds can be obtained from following relationship:

$$\sigma_{\bar{y}_{B-L}} = \sqrt{\int_0^{\infty} S_{f,B-L}(n) |H_1(n)|^2 dn} \quad (\text{A10})$$

where, $S_{f,B-L}(n)$ = wind force spectrum; $H(n)$ = transfer function. While the fluctuating component of gust-front winds is a nonstationary process being time-dependent, it necessitates the use of a time-dependent transfer function to evaluate the nonstationary RMS response.

Nonstationary random excitation has been generally assumed to be a product of an amplitude modulating function and a stationary process to obtain a closed-form solution; However, a closed-form solution is limited in some special cases, e.g., white-noise stationary and/or simple unit-step modulating function (e.g, Caughey and Stumpf 1961; Barnoski and Maurer 1969; Bucciarelli and Kuo 1970; Howell and Lin 1971; Corotis et al. 1972; Hasselman 1972; Holman and Hart 1974; Corotis and Marshall 1977; Michaelov et al. 1999a, b and 2001).

Two time-dependent transfer functions have been utilized in the evaluation of the nonstationary RMS response, e.g., a time-dependent impulse response function (TDIRF) (e.g., Barnoski and Maurer 1969; Bucciarelli and Kuo 1970; Corotis et al. 1972; Holman and Hart 1974; Corotis and Marshall 1977), and the other is a time-dependent frequency response function (TDFRF) (e.g., Howell and Lin 1971; Michaelov et al. 1999a, b and 2001). While TDIRF has the merit of obtaining a closed-form solution in some specific cases, this study utilizes TDFRF due to its simplicity in view of numerical analysis. Assuming that nonstationary random excitation $[f(t)]$ in a SDOF system is of the form:

$$f(t) = A(t) \cdot W(t) \quad (\text{A11})$$

where, $A(t)$ = amplitude modulating function (or envelop function); $W(t)$ = zero-mean Gaussian stationary process, then TDFRF [$M(n,t)$] can be expressed as

$$M(n,t) = \int_0^t h(t-\tau)A(\tau)e^{-i2\pi n(t-\tau)}d\tau \quad (\text{A12})$$

Due to the nature of the pulse-type time function used in this study, i.e., half-sine pulse (2), TDFRF for pulse-type modulating functions should be considered in two parts (Kwon and Kareem 2006b).

$$M(n,t) = \begin{cases} \int_0^t h(t-\tau)A(\tau)e^{-i2\pi n(t-\tau)}d\tau & 0 \leq t \leq t_d \\ \int_0^{t_d} h(t-\tau)A(\tau)e^{-i2\pi n(t-\tau)}d\tau & t \geq t_d \end{cases} \quad (\text{A13})$$

Note that the amplitude modulating function in Eq. (A11) becomes square of the half-sine function in this study since wind load is proportional to the square of the wind speed (Kwon and Kareem 2006b). For reference, closed-form solutions of TDFRF for very simple amplitude modulating functions can be found in Jangid (2004).

If the pulse duration (t_d) is long enough, TDFRF can be decomposed into a product of an amplitude modulating function and a time-independent transfer function (Howell and Lin 1971):

$$M(n,t) = \int_0^\infty h(t-\tau)A(\tau)e^{-i2\pi n(t-\tau)}d\tau \approx A(t) \cdot |H(n)|^2 \quad (\text{A14})$$

For distinctive purposes, this special case of TDFRF (A14) is denoted as time-independent frequency response function (TIFRF).

Nonstationary RMS response of fluctuating gust-front winds

In terms of TDFRF (A13) and one-sided fluctuating gust-front wind load spectrum (A9), nonstationary RMS displacement of the fluctuating gust-front wind can be obtained from following expression:

$$\sigma_{\bar{y}_{G-F}}(t) = \sqrt{\int_0^{\infty} S_{f,G-F}(n,t) |M(n,t)|^2 dn} \quad (\text{A15})$$

Since TDFRF generally becomes very complex, numerical integration is necessary. Note that TIFRF (A14) may be utilized instead of TDFRF (A13) in Eq. (A15) when the pulse duration (t_d) (2) is long enough for which a closed-form solution of the nonstationary RMS response exists and decomposition of nonstationary RMS response (A15) into background and resonant RMS responses akin to gust loading factor approach is viable (Kwon and Kareem 2006b).

To investigate the characteristics of the nonstationary RMS response of fluctuating gust-front winds, RMS responses in boundary layer winds and responses using TIFRF (TIFRF response) (A14) and TDFRF (TDFRF response) (A13) are used under following test conditions: $B = D = 40$ m, $H = 200$ m, $n_0 = 0.2$ Hz ($T_1 = 1/0.2 = 5$ sec), $\rho_B = 180$ kg/m³, $\rho_a = 1.25$ kg/m³, $\zeta_1 = 0.01$, $V_{3-s} = 40$ m/s, Criterion 2 (5b) and $t_d/T_1 = 1, 3$. In the case of a relatively short pulse duration ($t_d/T_1 = 1$), a transient response appears in the TDFRF response and its maximum is larger than the response in boundary layer winds and the maximum of the TIFRF response (Fig. A1a). As such, the TIFRF response fails to reveal transient characteristics of the nonstationary RMS response in short pulse duration since time characteristics of the TIFRF only depend upon an amplitude modulating function

(A14). Due to the nature of TDFRF and TIFRF (A13, A14), response in the free vibration part ($t \geq t_d$) only appears for the TDFRF response, while the TIFRF response remains zero (Fig. A1). This transient nature disappears for a longer pulse duration ($t_d/T_1 = 3$) and the maxima of the TIFRF and TDFRF responses become closer each other (Fig. A1b). Note that those maxima are smaller than the response in boundary layer winds since the pulse excitation occurs over a relatively short period ($t_d = 15$ sec), compared to the response in boundary layer winds in a 1-hour period. If a pulse duration becomes longer and longer, those maxima gradually approach the response in boundary layer winds (Kwon and Kareem 2006b).

NATHAZ Modeling Laboratory
University of Notre Dame

APPENDIX III. PEAK FACTOR IN GUST-FRONT WIND

Davenport (1964) suggested the following peak factor expression which was based on the approximation of the probability distribution of extreme value in stationary Gaussian processes, which has been widely used to estimate peak values under conventional boundary layer winds in most codes and standards:

$$g_{B-L} = \sqrt{2 \ln(v_0 T)} + \frac{0.5772}{\sqrt{2 \ln(v_0 T)}} \quad (\text{A16})$$

where, g_{B-L} = peak factor in stationary Gaussian process; T = duration (sec), typically taking 3,600 sec (1-hour); v_0 = cyclic rate ($\approx n_I$ in case of structural dynamic response); n_I = natural frequency of structure.

While the peak factor in nonstationary processes, such as gust-front winds, is also time-dependent in the strict sense, for practical application, this study utilizes the mean peak factor (g_{G-F}) instead of time-dependent peak factor [$g_{G-F}(t)$]. In this manner, g_{G-F} can be expressed similar to the conventional peak factor in a stationary process (A16) utilizing respective equivalent parameters (Michaelov et al. 2001):

$$g_{G-F} = \sqrt{2 \ln(2v_0 T_{eq})} + \frac{0.5772}{\sqrt{2 \ln(2v_0 T_{eq})}} \quad (\text{A17})$$

$$T_{eq}^2(T, P) = \exp[n(T, P)] \int_0^T \exp\left(-\frac{n(T, P) \sigma_{eq}^2[n(T, P)]}{\sigma_{\dot{y}_{G-F}}^2(t)}\right) dt \quad (\text{A18})$$

$$\sigma_{eq}^2(n) = \frac{I(n+1)}{I(n)}, \quad I(n) = \int_0^T \sigma_{\dot{y}_{G-F}}^{2n}(t) dt$$

where, T_{eq} = equivalent time interval of process; σ_{eq} = equivalent standard deviation of extreme value; $n = 2$. The cyclic rate ν_0 in nonstationary processes is also time-dependent and is expressed as

$$\nu_0(t) = \frac{1}{2\pi} \sqrt{1 - \rho_{\dot{y}_{G-F}, \dot{y}_{G-F}}^2(t)} \frac{\sigma_{\dot{y}_{G-F}}(t)}{\sigma_{\ddot{y}_{G-F}}(t)} \quad (A19)$$

where, $\rho_{\dot{y}_{G-F}, \dot{y}_{G-F}}(t)$ = correlation coefficient. For simplicity, it is assumed that

$$\rho_{\dot{y}_{G-F}, \dot{y}_{G-F}}(t) \approx 0 \text{ and } \sigma_{\dot{y}_{G-F}}(t) / \sigma_{\ddot{y}_{G-F}}(t) \approx \omega_0 \text{ (Michaelov et al. 2001), therefore, } \nu_0(t) \text{ (A19)}$$

becomes $\nu_0 \approx n_I$ as treated in a stationary process (A16). Note that numerical integrations are still inevitable to calculate both σ_{eq} and T_{eq} (A18). More details can be found in Michaelov et al. 2001 and Kwon and Kareem 2006b.

NATHAZ Modeling Laboratory
University of Notre Dame

APPENDIX IV. STORM-TRANSLATION EFFECT FACTOR, I_{s-m}

Storm-translation effect factor (I_{s-m}) (17, 24) can be analytically derived as follows.

$$I_{s-m} = \frac{y_{s-m}}{\max[\bar{y}_{G-F}(z, t)]} = \frac{\frac{1}{K_1} \frac{1}{2} \rho_a B \int_0^H V_{s-m}^2 \phi_1(z) dz}{\left(\frac{1}{K_1} \frac{1}{2} \rho_a B \int_0^H V_{G-F}^2(z) \phi_1(z) dz \right) \cdot I_2} = \frac{0.2727}{J_0 \cdot I_2} \left(\frac{V_{s-m}}{V_{max}} \right)^2 \quad (A20)$$

where, $J_0 = \text{Eq. (A6)}$; $I_2 = \text{pulse dynamics factor (19, 22)}$. In this manner, the storm-translation effect on a building depends on the storm-translation speed (V_{s-m}), pulse duration (t_d) due to the I_2 factor and building height (H) due to J_0 . Thus, the I_{s-m} factor becomes smaller in short pulse duration as compared to long pulse duration for a given building height as transient effects generally occur in short pulse duration where factor I_2 (19, 22) becomes larger than unity (e.g., Table 2). In addition, it is obvious that the effect of a fast storm-translation speed on a building will be larger than slower speed, which is well described in this expression since factor I_{s-m} is proportional to square of storm-translation speed (V_{s-m}). In most cases, factor I_{s-m} is small since V_{max} (Table 1) is generally several times larger than V_{s-m} , which is generally assumed to be 10~20 m/s (e.g., Holmes and Oliver 2000; Letchford and Chay 2002).

FIGURE CAPTIONS:

Fig. 1. Time functions in gust-front winds; (a) Wind record of the Andrew AFB downburst at 4.9 m height (Fujita 1985); (b) Full-scale data (RFD) (Gast and Schroeder 2003) and its time-varying mean (Wang and Kareem 2004); (c) Half-sine pulse

Fig. 2. Profile criteria; (a) Criterion 1 : $V_{G-F}(10) = V_{B-L}(10)$; (b) Criterion 2 : $V_{max} = V_{B-L}(z_G)$

Fig. 3. Schematic diagram of gust-front factor framework

Fig. 4. Practical consideration of F_{Design}

Fig. 5. F_{ASCE7} and F_{Final} in exemple buildings ($t_d = 200$ sec) [1) $B = D = 20$ m, $H = 60$ m, $n_l = 0.8$ Hz ($T_l = 1.25$ sec); 2) $B = D = 20$ m, $H = 100$ m, $n_l = 0.4$ Hz ($T_l = 2.5$ sec); 3) $B = D = 40$ m, $H = 200$ m, $n_l = 0.2$ Hz ($T_l = 5$ sec)]; (a) Criterion 1, exposure B; (b) Criterion 1, exposure C; (c) Criterion 2, exposure B; (d) Criterion 2, exposure C

Fig. 6. Web-based on-line gust-front factor framework : User-friendly interface

Fig. 7. Web-based on-line gust-front factor framework : Results interface

Fig. A1. An example of nonstationary RMS responses (B-L: response in boundary layer winds; TIFRF : response using TIFRF in gust-front winds; TDFRF : response using TDFRF in gust-front winds); (a) $t_d/T_l = 1$; (b) $t_d/T_l = 3$

TABLE CAPTIONS:

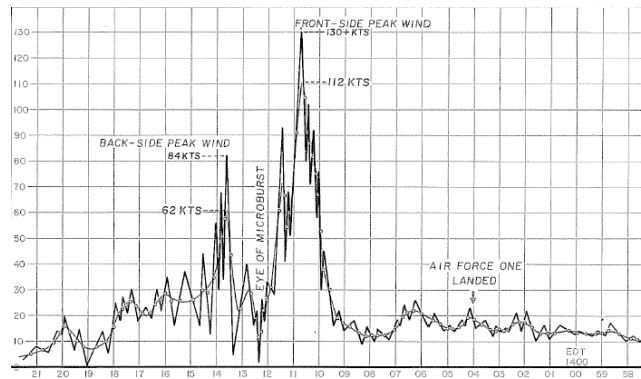
Table 1. V_{max} and z_{max} for terrain exposures (V_{3-s} is assumed as 40 m/s)

Table 2. Factor I_2 versus the ratio of t_d/T_1

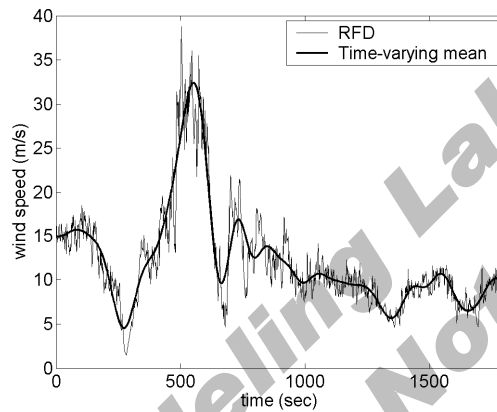
Table 3. Gust-front factor (G_{G-F}): kinematic effects (I_1) and dynamic effects (I_2, I_3, I_4) on buildings in exposure B ($I_4 = 1.0$)

Table 4. Gust-front factor (G_{G-F}): kinematic effects (I_1) and dynamic effects (I_2, I_3, I_4) on buildings in exposure C ($I_4 = 1.0$)

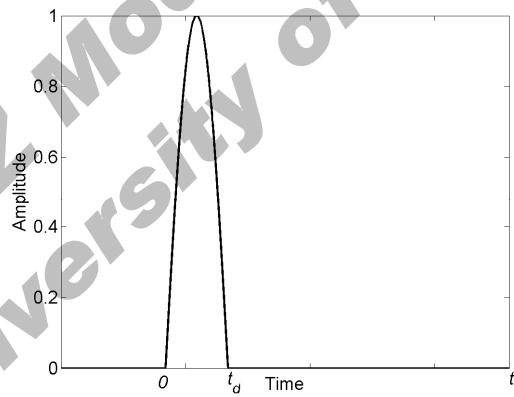
NATHAZ Modeling Laboratory
University of Notre Dame



(a)

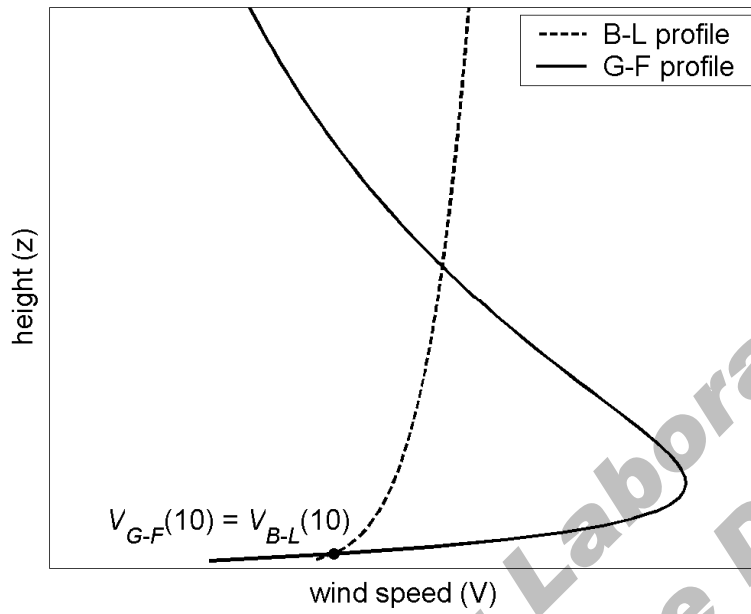


(b)

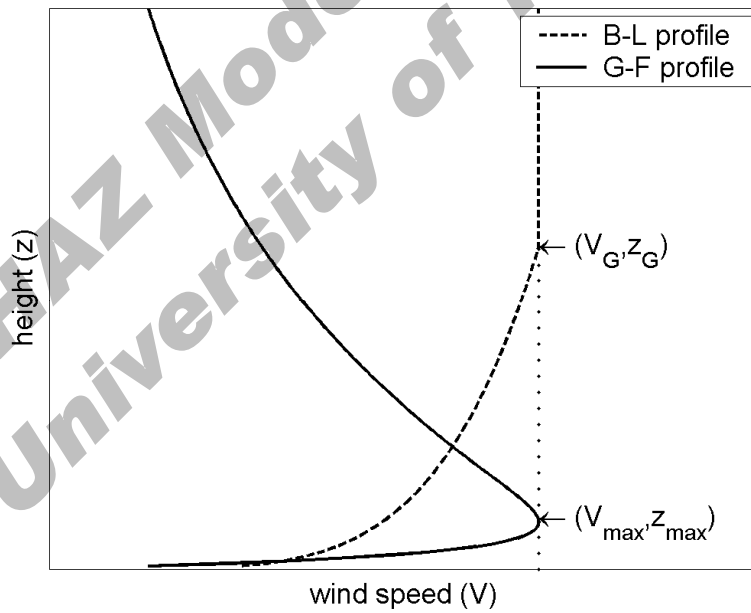


(c)

Fig. 1. Time functions in gust-front winds; (a) Wind record of the Andrew AFB downburst at 4.9 m height (Fujita 1985); (b) Full-scale data (RFD) (Gast and Schroeder 2003) and its time-varying mean (Wang and Kareem 2004); (c) Half-sine pulse



(a)



(b)

Fig. 2. Profile criteria; (a) Criterion 1 : $V_{G-F}(10) = V_{B-L}(10)$; (b) Criterion 2 : $V_{max} = V_{B-L}(z_G)$

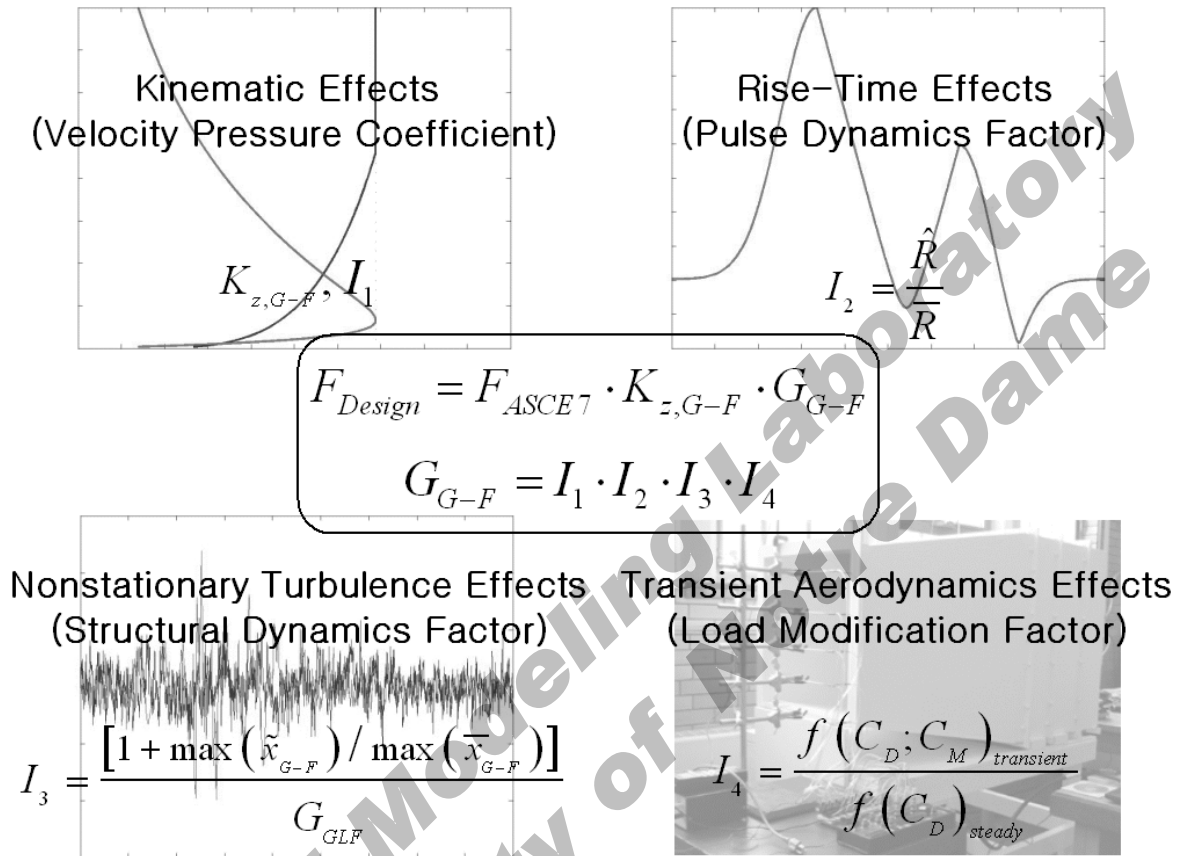


Fig. 3. Schematic diagram of gust-front factor framework

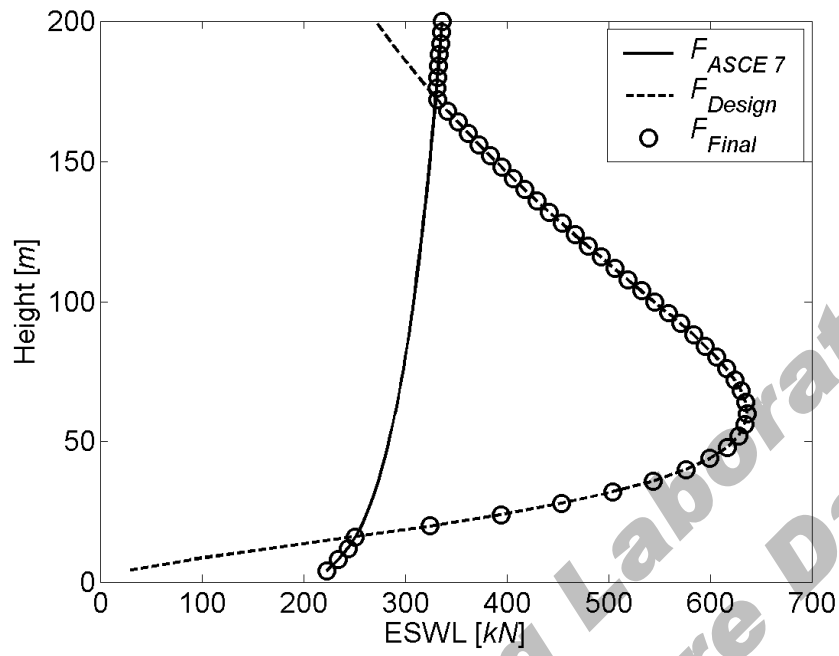
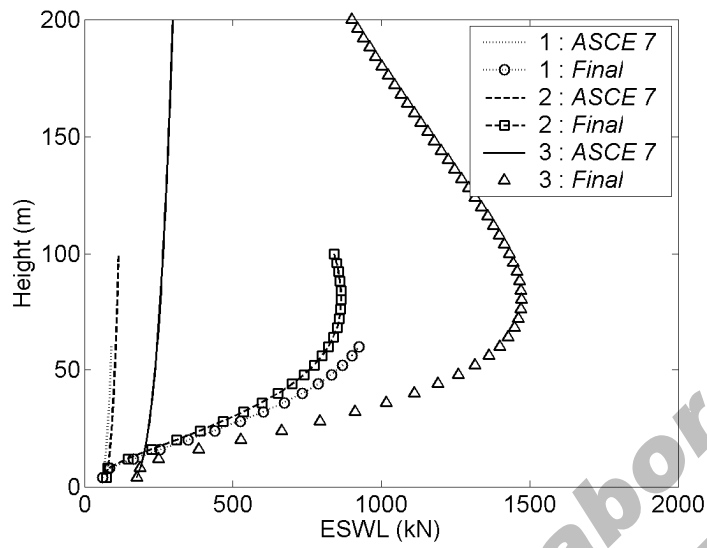
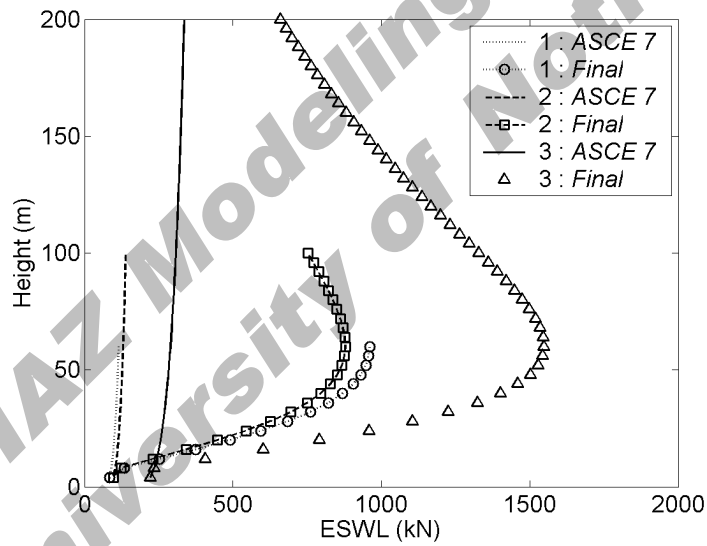


Fig. 4. Practical consideration of F_{Design}

NATHAZ Modeling Laboratory
 University of Notre Dame

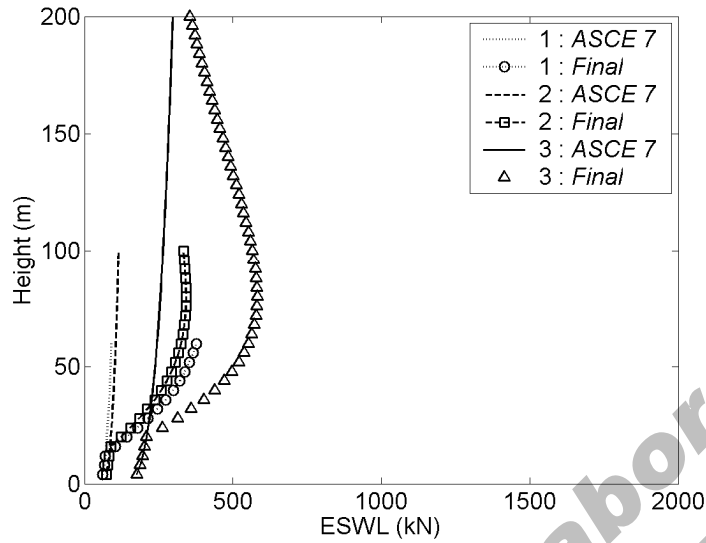


(a)

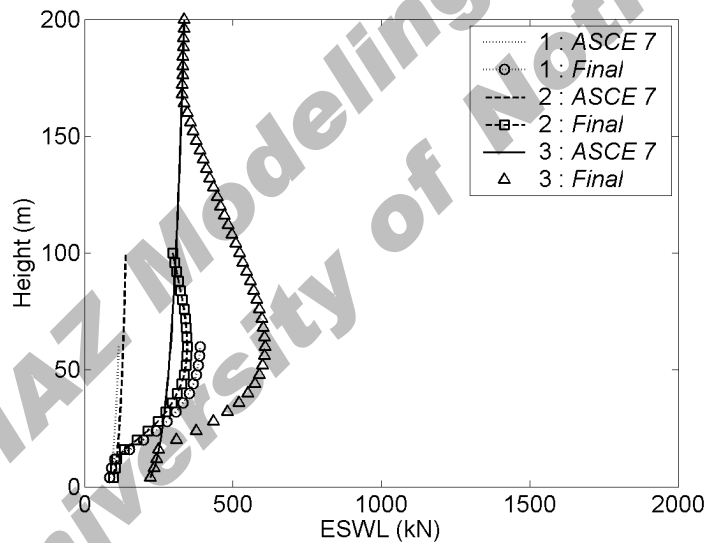


(b)

Fig. 5.



(c)



(d)

Fig. 5. F_{ASCE7} and F_{Final} in exemple buildings ($t_d = 200$ sec) (continue) [1) $B = D = 20$ m, $H = 60$ m, $n_l = 0.8$ Hz ($T_l = 1.25$ sec); 2) $B = D = 20$ m, $H = 100$ m, $n_l = 0.4$ Hz ($T_l = 2.5$ sec); 3) $B = D = 40$ m, $H = 200$ m, $n_l = 0.2$ Hz ($T_l = 5$ sec)]; (a) Criterion 1, exposure B; (b) Criterion 1, exposure C; (c) Criterion 2, exposure B; (d) Criterion 2, exposure C



■ Please select the unit of input values (default : Metric) [On-line Unit Converter]
 If user would like to see English unit output, please select checkbox (default : Metric)

Metric(SI) unit [kg, m, m/s]
 English unit [lb, ft, mph]
 Output : English unit

■ Building width B , depth D and height H

B [m, ft]
 D [m, ft]
 H [m, ft]

■ 1st frequency for alongwind f_x , Mode shape exponent β , Floor-to-floor height of building ΔH

f_x [Hz]
 β
 ΔH [m, ft]

■ Bulk Density ρ_B , Air density ρ_a , Damping ratio of building ζ

ρ_B [kg/m³, lb/ft³]
 ρ_a [kg/m³, lb/ft³]
 ζ

■ Pulse duration t_d , 3-second basic wind speed in ASCE 7 V_{3-S} , storm-moving speed V_{s-m}

t_d [sec]
 V_{3-S} [m/s, mph]
 V_{s-m} [m/s, mph]

■ Exposure Category (A,B,C,D based on ASCE 7) & Select checkbox if building is located in Alaska

A
 B
 C
 D
 Alaska

■ Category selection for Importance factor I (I, II, III, IV in Table 1-1 of ASCE 7) : Default is II ($I = 1.0$)

I
 II (Default)
 III
 IV

■ Velocity relationship between gust-front wind and ABL wind : Vicroy (1991) model is being used
 Third option is user-defined inputs of V_{max} [m/s, mph] and z_{max} [m, ft], e.g., 67,67 or 67 67

$V_{G-F}(10) = V_{BL}(10)$
 $V_{max,G-F} = V_{BL}(z_G)$
 $V_{max} z_{max}$

Design/analysis options

- Gust-front factor approach in gust-front wind (Default)
- ASCE 7 design procedure in boundary-layer wind

Fig. 6. Web-based on-line gust-front factor framework : User-friendly interface

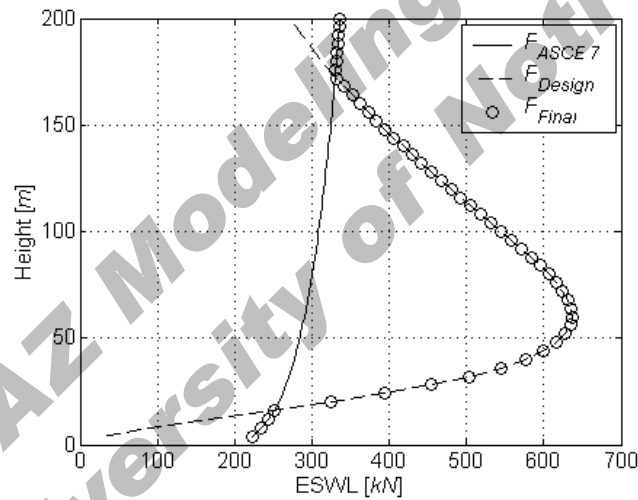
■ Input parameters by user

B	40 m	D	40 m	H	200 m
f_x	0.2 Hz	β	1	ΔH	4 m
ρ_B	180 kg/m ³	ρ_a	1.225 kg/m ³	ζ	0.01
t_d	200 sec	V_{3-s}	40 m/s	V_{s-m}	12 m/s
Exposure C		$V_{max,G-F} = V_{B-L,3-s}(z_G)$			
Input unit : Metric (SI)		Output unit : Metric (SI)		[On-line Unit Converter]	

■ Gust-front factor : $G_{G-F} = I_1 \cdot I_2 \cdot I_3 \cdot I_4$, total dynamic effects = $I_2 \cdot I_3 \cdot I_4$ ($I_4 = 1.0$)

I_1	I_2	I_3	I_4	$I_2 \cdot I_3 \cdot I_4$	G_{G-F}
1.348	1.000	0.853	1.000	0.853	1.150

■ Equivalent static wind loads (ESWL) : $F_{ASCE 7}$, F_{Design} and F_{Final}

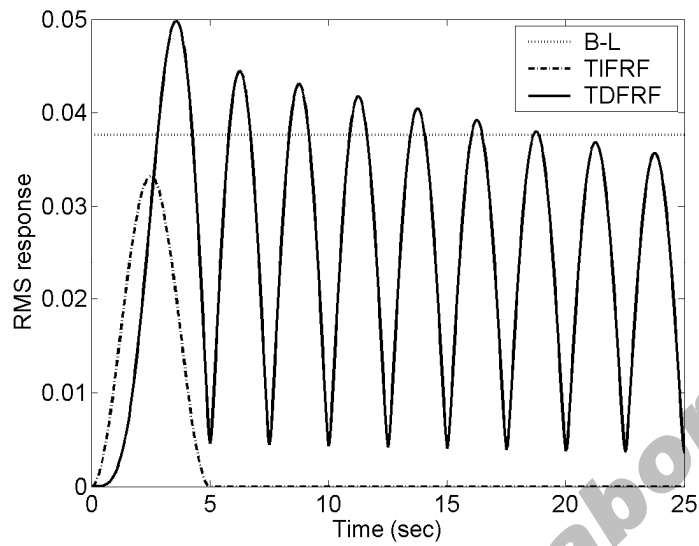


(F_{Final} is taken as larger design load (ESWL) between $F_{ASCE 7}$ and F_{Design} at each interstory height.)

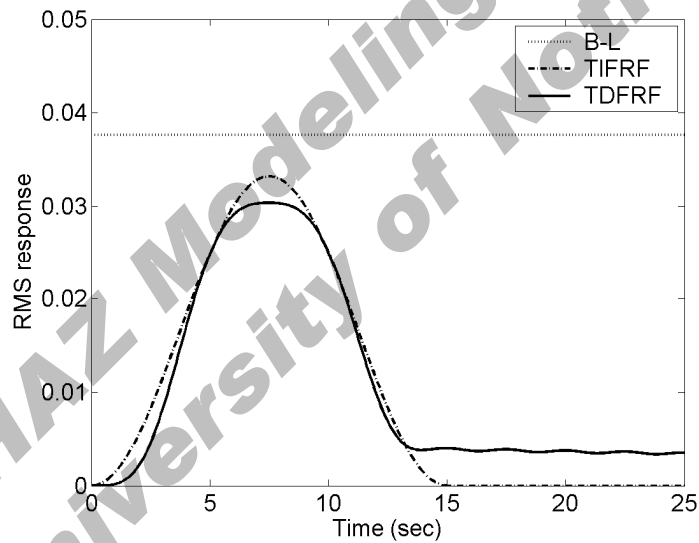
■ Download data file of Design wind loads : GFF_out_all_m100039.dat

(Col. 1 : Height [m], Col. 2 : $F_{ASCE 7}$ [kN], Col. 3 : F_{Design} [kN], Col. 4 : F_{Final} [kN])

Fig. 7. Web-based on-line gust-front factor framework : Results interface



(a)



(b)

Fig. A1. An example of nonstationary RMS responses (B-L: response in boundary layer winds; TIFRF : response using TIFRF in gust-front winds; TDFRF : response using TDFRF in gust-front winds); (a) $t_d/T_1 = 1$; (b) $t_d/T_1 = 3$

Table 1. V_{max} and z_{max} for terrain exposures (V_{3-s} is assumed as 40 m/s)

	V_{max} [m/s]		z_{max} [m]
	Criterion 1	Criterion 2	
exposure A	71.26	45.15	100.58
exposure B	81.29	51.50	80.47
exposure C	89.47	56.68	60.35
exposure D	93.06	58.96	46.94

NATHAZ Modeling Laboratory
 University of Notre Dame

Table 2. Factor I_2 versus the ratio of t_d/T_1

t_d/T_1	$n_0 = 0.8$ Hz ($T_1 = 1.25$ sec)	$n_0 = 0.4$ Hz ($T_1 = 2.5$ sec)	$n_0 = 0.2$ Hz ($T_1 = 5.0$ sec)
0.5	1.313	1.313	1.313
1.0	1.681	1.681	1.681
2.0	1.323	1.323	1.323
3.0	1.006	1.006	1.006
4.0	1.063	1.063	1.063
5.0	1.003	1.003	1.003
6.0	1.026	1.026	1.026
7.0	1.002	1.002	1.002
8.0	1.014	1.014	1.014

NATHAZ Modeling Laboratory
University of Notre Dame

Table 3. Gust-front factor (G_{G-F}): kinematic effects (I_1) and dynamic effects (I_2, I_3, I_4) on buildings in exposure B ($I_4 = 1.0$)

Building	t_d [sec]	Criterion 1				G_{G-F}	Criterion 2				
		I_1	I_2	I_3	$I_2 \cdot I_3 \cdot I_4$		I_1	I_2	I_3	$I_2 \cdot I_3 \cdot I_4$	G_{G-F}
1	5	6.36	1.06	0.83	0.88	5.57	2.55	1.06	0.84	0.90	2.29
	10		1.01	0.89	0.90	5.74		1.01	0.91	0.92	2.35
	100		1.00	1.06	1.06	6.70		1.00	1.07	1.07	2.73
	200		1.00	1.10	1.10	6.97		1.00	1.11	1.11	2.83
2	5	6.54	1.32	0.73	0.96	6.29	2.63	1.32	0.74	0.98	2.58
	10		1.06	0.75	0.80	5.20		1.06	0.76	0.81	2.13
	100		1.00	0.91	0.91	5.95		1.00	0.92	0.92	2.41
	200		1.00	0.95	0.95	6.21		1.00	0.95	0.95	2.51
3	5	4.55	1.68	0.73	1.22	5.57	1.83	1.68	0.74	1.24	2.27
	10		1.32	0.66	0.88	3.98		1.32	0.69	0.91	1.65
	100		1.00	0.78	0.78	3.55		1.00	0.79	0.79	1.44
	200		1.00	0.81	0.81	3.70		1.00	0.82	0.82	1.50

Table 4. Gust-front factor (G_{G-F}): kinematic effects (I_1) and dynamic effects (I_2, I_3, I_4) on buildings in exposure C ($I_4 = 1.0$)

Building	t_d [sec]	Criterion 1				G_{G-F}	Criterion 2				
		I_1	I_2	I_3	$I_2 \cdot I_3 \cdot I_4$		I_1	I_2	I_3	$I_2 \cdot I_3 \cdot I_4$	G_{G-F}
1	5	5.86	1.06	0.85	0.90	5.28	2.35	1.06	0.86	0.92	2.16
	10		1.01	0.90	0.91	5.35		1.01	0.92	0.93	2.19
	100		1.00	1.04	1.04	6.06		1.00	1.05	1.05	2.46
	200		1.00	1.07	1.07	6.26		1.00	1.08	1.08	2.54
2	5	5.47	1.32	0.76	1.00	5.47	2.20	1.32	0.77	1.02	2.24
	10		1.06	0.78	0.83	4.53		1.06	0.79	0.84	1.85
	100		1.00	0.91	0.91	4.99		1.00	0.92	0.92	2.01
	200		1.00	0.95	0.95	5.18		1.00	0.95	0.95	2.08
3	5	3.36	1.68	0.77	1.29	4.33	1.35	1.68	0.78	1.31	1.76
	10		1.32	0.71	0.94	3.14		1.32	0.73	0.97	1.31
	100		1.00	0.82	0.82	2.75		1.00	0.83	0.83	1.12
	200		1.00	0.85	0.85	2.85		1.00	0.85	0.85	1.15